

Perspective on spin-based wave-parallel computing



Cite as: Appl. Phys. Lett. **123**, 190502 (2023); doi: [10.1063/5.0168083](https://doi.org/10.1063/5.0168083)

Submitted: 17 July 2023 · Accepted: 26 September 2023 ·

Published Online: 6 November 2023



[View Online](#)



[Export Citation](#)



[CrossMark](#)

Makoto Kohda,^{1,2,3,4,a)} Takeshi Seki,⁵ Yasushi Yuminaka,⁶ Tetsuya Uemura,⁷ Keito Kikuchi,¹ and Gian Salis⁸

AFFILIATIONS

¹Department of Materials Science, Tohoku University, Sendai 980-8579, Japan

²Center for Science and Innovation in Spintronics (Core Research Cluster), Tohoku University, Sendai 980-8577, Japan

³Division for the Establishment of Frontier Science, Tohoku University, Sendai 980-8577, Japan

⁴Quantum Materials and Applications Research Center, National Institute for Quantum Science and Technology, Gunma 370-1292, Japan

⁵Institute for Materials Research, Tohoku University, Sendai 980-8577, Japan

⁶Graduate School of Science and Technology, Gunma University, Gunma 376-8515, Japan

⁷Graduate School of Information Science and Technology, Hokkaido University, Sapporo 060-0814, Japan

⁸IBM Research-Zurich, Säumerstrasse 4, 8803 Rüschlikon, Switzerland

^{a)}Author to whom correspondence should be addressed: makoto.koda.c5@tohoku.ac.jp

ABSTRACT

Waves exhibit unique characteristics, such as diffraction and interference, which distinguishes them from the particle nature of electrons currently used for binary and sequential data processing and storage. In the solid state, wave properties can be found in electron spin waves in semiconductors or magnons in magnetic materials. These are useful for communication, processing and storage, and allow multiplexing of the information. Given this perspective, after introducing the information theory of wave-parallel computing and arguing the fundamental properties necessary for implementation with wave-based information carriers, we specifically examine how electron spin waves and magnons can be used as information carriers for processing and storage. Then, after explaining the fundamental physics of the electron spin wave based on the persistent spin helix state, we assess the potential of magnon-assisted magnetization switching for realizing the selective writing and reading of multiplexed information. Ferromagnet/semiconductor hybrid structures are emphasized as a platform for generating and controlling both electron spin waves and magnons. Interconversion among light helicity, electron spin waves and magnons is also discussed. Finally, we show several challenges and provide an outlook on the key steps that must be demonstrated for implementing spin-based wave-parallel computing.

© 2023 Author(s). All article content, except where otherwise noted, is licensed under a Creative Commons Attribution (CC BY) license (<http://creativecommons.org/licenses/by/4.0/>). <https://doi.org/10.1063/5.0168083>

I. INTRODUCTION

Spintronics uses electrons' spin degrees of freedom in semiconductors¹ and magnetic materials as information carriers.^{2,3} Using spin polarized states, information processing and nonvolatile storage have been developed for low-power integrated circuits⁴ and magnetic random-access memory (MRAM).⁵ Two spin states, spin up and spin down, are compatible with a binary systems with Boolean logic. Moreover, the non-volatility of the magnetic moment is beneficial for power consumption. Such spin states in ferromagnets and semiconductors can be controlled through spatially uniform spin flow: the so-called spin current.⁶ During the past two decades, efficient generation,

manipulation, and detection of the spin currents have been important achievements for the development of various spin functionalities in spintronics.^{1–5}

Spatial spin textures are expected to play a crucially important role in quantum and topological phenomena and for information carriers. In ferromagnetic materials, magnetic moments form various spatial structures as a stationary state, consequently leading to the emergence of topological effects and states known as the topological Hall effect,^{7,8} chiral domain wall,^{9,10} Skyrmion,^{11,12} and chiral-spin rotation.¹³ Spin dynamics in ferromagnetic materials, such as the collective precessional motion of local magnetic moments, possess a wave

nature for which the elementary excitation is the so-called magnon.¹⁴ Because of well-established nanoscale device fabrication and matured growth techniques used for various magnetic thin films, magnetic spin wave-based logic operation by controlling the amplitude and phase of the wave has been studied intensively.¹⁵ Here, we define the collective motion of a local magnetic moment as the magnetic spin wave, which we distinguish from an electron spin wave defined by the spatial rotation of electron spins.

Among various logic devices, implementations of majority gates are of particular interest because of the possible realization of Boolean logic using simpler and more compact circuit designs than CMOS gates.^{16–28} For this scheme, magnetic spin waves with identical frequency and wavelength are excited as inputs, mutually interfered, and finally detected. In the majority gate, three magnetic spin waves mutually interfere. Depending on whether the interference is destructive or constructive, the output state is defined as the majority among three magnetic spin waves. By combining the majority gate with an inverter, various logic operations can be realized, such as a half adder.²⁹ Consequently, a new computing paradigm can be expected based on the nature of magnetic spin waves. Nevertheless, several challenges remain, such as cascading, fan-out, signal restoration, transducer efficiency, and device scaling in magnetic spin wave-based circuits.³⁰ Integration with optical communications will also necessitate their combination with light emitting devices and photodiodes.

In semiconductors, electron spins also form a spin wave as electron spins rotate around an effective magnetic field induced by spin-orbit (SO) interaction.^{31–33} The SO interaction is well known to randomize the spin state generally, causing spin relaxation.³⁴ However, when the effective magnetic fields are aligned in a uniaxial orientation with spin SU(2) symmetry,³⁵ the spin relaxation is suppressed. Yet, the spatial spin precession is maintained.³⁶ This particular condition leads to emergence of a persistent spin helix (PSH) state,^{37–39} enabling the stable excitation and control of electron spin waves in semiconductors.^{40,41} The electron spin wave can propagate over 100 μm by drift current;⁴² its phase is either modulated or locked during spatial propagation.⁴³ The wavelength, which varies from a few tens of nanometers to several tens of micrometers, depending on the material,^{40,41,44–52} is also controllable by an external gate.⁴⁰ Among various material systems, a III-V semiconductor heterostructure is an ideal platform for

using electron spin waves because of the strong SO interaction and optimal opto-electric integration such as with light emitting diodes and high-electron mobility transistors. Optical selection rules⁵³ and spin transfer torque⁵⁴ in III-V semiconductors connect light helicity, electron spin orientation, and local magnetic moment through interconversion of spin angular momentum. As presented in Table I, electron spin waves and magnetic spin waves (magnon) share similar characteristic scales of wavelength, lifetime, velocity, and propagation length, being advantageous for their interconversion. Typical wavelengths for electron spin wave in III-V and II-VI quantum wells are around 5 μm,^{40,48} which are comparable to those of thin YIG, Permalloy, and CoFeB.⁵⁵ The lifetime of magnetic spin waves is governed by the Gilbert damping parameter, whereas that of electron spin waves is determined by the SO interaction parameters, both of which reach a few nanoseconds. The YIG shows an exception attributable to a minimal damping parameter.⁵⁵ The spin wave velocity is a few to tens of kilometers per second both in semiconductors and magnetic materials. Information can be encoded using the amplitude, phase, wavelength, and frequency of waves and can be shared among light helicity, electron spin waves, and magnetic spin waves, as presented in Fig. 1(a), suggesting potential applications on seamless communication, computation, and storage using wave-based information carriers.

In this perspective, we specifically explain the use of physical properties of electron spin waves for implementing wave-based parallel information processing. Moreover, we review the information theory of wave-parallel computing and the latest reported research investigating electron spin waves in III-V semiconductors and magnetic spin wave-assisted magnetization switching toward wave-based information processing and storage. This perspective also includes the crystal growth of ferromagnet/semiconductor hybrid structures as a material platform. First, we discuss how wave-based computing differs from conventional binary circuits and its advantages from an information theory viewpoint. Then, we summarize the functions of the logic gates which are necessary to enable general-purpose parallel computing. Next, we describe the necessary properties of electron spin waves to realize these logic gates and introduce the principle of multiplexed information storage based on magnetic spin waves. After that, we describe the growth of a GaAs/Heusler alloy hybrid structure: an ideal platform for generating and controlling both electron spin waves and

TABLE I. Comparison of electron spin wave and magnetic spin wave parameters (wavelength, propagation velocity, propagation length, and lifetime) in GaAs⁴⁰ and CdTe⁴⁸ quantum wells (QWs) for electron spin wave and thick (5 nm) and thin (20 nm) yttrium-iron-garnet (YIG), Permalloy, and CoFeB for magnetic spin wave (magnon). For magnetic spin waves, parameters were referred from Table VI.1 of an earlier report.⁵⁵ Propagation velocity v is defined by the group velocity for magnons and by the drift velocity with given electric field ($E = 1 \text{ kV/m}$) for electron spin wave. The spin wave lifetime τ is defined by the Gilbert damping parameter for magnon and by time-resolved Kerr rotation microscopy for electron spin wave. The propagation length is defined by $v \times \tau$. Adapted from Chumak *et al.*, J. Phys. D: Appl. Phys. **50**, 244001 (2017). Copyright 2017 Author(s), licensed under a Creative Commons Attribution (CC BY) license.

	Electron spin wave		Magnetic spin wave (Magnon)			
	GaAs QW	CdTe QW	Thick YIG	Thin YIG	Permalloy	CoFeB
Wavelength (μm)	5.7	5.6	314	1.26	1.29	1.27
Propagation velocity (km/s)	15	42	33.7	0.23	2.0	3.5
	@ $E = 1 \text{ kV/m}$		@ $t = 51 \mu\text{m}$	@ $t = 20 \text{ nm}$	@ $t = 20 \text{ nm}$	@ $t = 20 \text{ nm}$
Propagation length (μm)	15	56.7	20.4	35.1	2.7	5.7
Lifetime (ns)	1.0	1.35	604.9	150.2	1.3	1.6
	@4.77 GHz		@4.8 GHz	@11.1 GHz	@14.9 GHz	

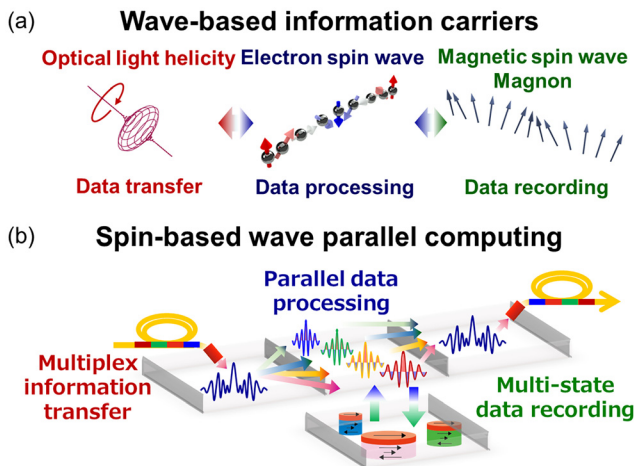


FIG. 1. (a) Optical light helicity, electron spin wave, and magnetic spin wave (magnon) as wave-based information carriers for data transferring, processing, and storage. Multiplexity and parallelism in each wave-based information carrier can be shared by spin angular momentum, enabling the efficient interconversion. (b) Schematic illustration of spin-based wave-parallel computing. Multiplexed information is transferred from light helicity to multiplexed electron spin waves in a semiconductor. Parallel data processing is conducted by multiplex electron spin waves, then storage as multi-state data through magnetic spin wave (magnon)-assisted magnetization switching.

magnetic spin waves, and for spin injection into a two-dimensional electron gas. Finally, interconversion among light, electron spin waves, and magnetic spin waves is also discussed to share the wave-based information in communication, processing, and storage. Then, we provide a conclusion and some prospects for necessary future technological developments.

II. WAVE-PARALLEL COMPUTING CONCEPT

Currently, multi-valued data representation using multi-level signals, such as 4-valued (2 bits/cell), 8-valued (3 bits/cell), etc., is being used for increasing the information density of flash memory.⁵⁶ Multi-level information, i.e., r -valued representation, increases the information

capacity by encoding $\log_2(r)$ bits to r values. Operating multiple binary (two-valued) circuits in parallel can also be achieved by encoding them on multi-valued signals. For instance, four parallel OR operations of conventional binary logic presented in Fig. 2(a) can be realized in a single gate on two multi-valued inputs. A multi-level OR operation is calculated as a bitwise OR operation of each bit. However, this requires multi-valued signals of $2^4 = 16$ levels. Such scaling is not advantageous from the perspective of noise margin at low-voltage operations.

To address these issues, parallel information processing based on the “information multiplexing” concept was proposed in the 1990s.⁵⁷ The proposed system of a framework of logic functions called “set-valued logic” has been constructed to replace the existing digital logic functions.⁵⁸ Based on this idea, Yuminaka *et al.* have proposed a model of wave-parallel computing, which is an ideal parallel processing method using the parallelism and multiplicity of waves.⁵⁹ The fundamental concept is “multiplexing of logic values,” which is aimed at increasing the density of information per line by multiplexing logic values in multiple dimensions. Specifically, by representing information according to the presence or absence of information carriers of r kinds, the number of available states is increased to 2^r , allowing the encoding of r bits by r parallel waves. This is a core concept of wave-parallel computing, which is distinguished from conventional binary and multi-valued logic. As presented in Fig. 2(b), independent and non-interacting information carriers, e.g., those with distinct frequency f_i , can be multiplexed and can exist in parallel. A single circuit on four parallel waves $\{f_1, f_2, f_3, f_4\}$ can perform parallel computations of four OR operations at once. This system, therefore, employs the frequency space for parallel processing. The principle of parallel computing is simple, yet it enables us to reduce the number of interconnections among modules to $1/r$ of the original binary circuits.⁵⁹ It is noteworthy that the wave-parallel computing uses both the multiplicity and parallelism of waves simultaneously.

To construct a highly parallel logic system based on such a logic-valued multiplexing concept, the choice of the information carrier is an important consideration. Information carriers must be stable as waves and must propagate over long distances. At the same time, they must be able to be mixed and multiplexed simultaneously without mutually interacting in the transmission medium. Moreover, they must be selectively separable and detectable by some means.

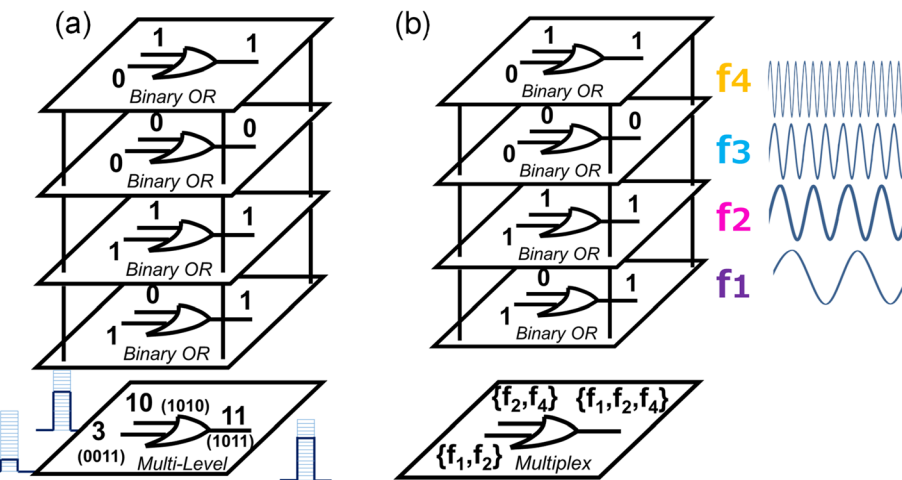


FIG. 2. Conceptual overview of wave-parallel computing of four OR operations by comparing with conventional binary OR operation. (a) Four OR operations with conventional binary logic and equivalent logic operation based on multi-valued signal of 16 levels. (b) Wave-parallel computing with four different frequencies (f_1, f_2, f_3 , and f_4), which is equivalent to binary-based four OR operations.

Considering affinity with current integrated circuits, the frequency of electrical signals⁵⁹ or the wavelength of optical signals propagating in a waveguide⁵⁷ would be suitable to encode information related to wave carriers. As explained later, an electron spin wave is an ideal information carrier to implement wave-parallel computing in conventional semiconductor devices.

To construct wave-parallel computing systematically, we have established an algebraic framework for wave-parallel computing.^{57,59} A single 2^r -valued circuit can simulate r independent binary circuits simultaneously as if there were r binary functions operating in parallel using the parallelism of multiplexable information carriers. In this system, multiplexed binary signals are treated as a “set” of information carriers. For instance, wave-parallel computing of four OR functions [Fig. 2(b)] can be represented conveniently as a set-theoretic union operation: $\{f_1, f_2\} \cup \{f_2, f_4\} = \{f_1, f_2, f_4\}$.

Conventional binary circuits use binary variables for which two values are represented by the bits 0 or 1. The circuits perform binary logic functions of n input variables defined as a mapping $g: \{0, 1\}^n \rightarrow \{0, 1\}$. By contrast, wave-parallel computing uses a set of r kinds of information carriers $L = \{c_1, c_2, c_3, \dots, c_r\}$ to handle information. Functions between sets are defined as a mapping $G: (2^L)^n \rightarrow 2^L$, where 2^L is the power set of L defined as $2^L = \{X | X \subseteq L\}$.

To realize wave-parallel computing, we have proposed basic building blocks of three kinds that perform switching of multiplexed information carriers directly.⁵⁹ The building block symbols are shown, respectively, in Figs. 3(a)–3(c) as set-difference (SD), set-generation (SG), and union (U) gates. These three blocks are a functionally complete set of gates, i.e., universal gates, meaning that every possible parallel logic gate can be realized using the SD, SG, and U gates.⁵⁸ The SD gate selects a specific set of information carriers selectively from the input set. The SG gate produces a specific set of information carriers. The U gate performs a set-theoretic union operation.

As one example, letting $L = \{f_1, f_2\}$, then one can consider two binary functions: $y_1 = g_1(x_1, x_2) = \overline{x_1 + x_2}$ (NOR) and $y_2 = g_2(x_3, x_4) = \overline{x_3 \cdot x_4}$ (NAND). The table of combinations of these functions is presented as Table II. Two binary variables are multiplexed into a single set-valued variable according to the mapping $X_1 = \varphi(x_1, x_2)$, $X_2 = \varphi(x_3, x_4)$, and $Y = \varphi(y_1, y_2)$. Here, function φ is a mapping function that maps the binary bit of 1 and 0 into a set of presence or absence of frequency components. Table II can be rewritten using set-valued variables as Table III.

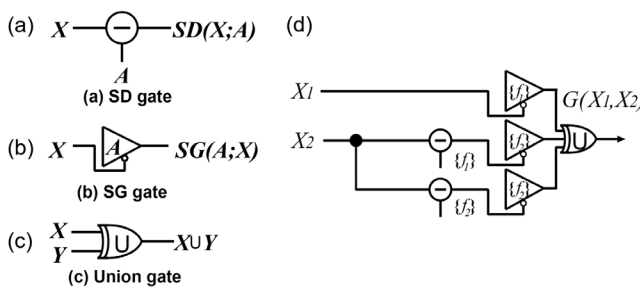


FIG. 3. Symbols of basic building blocks for wave-parallel computing. (a) Set-Difference (SD) gate, (b) Set-Generation (SG) gate, and (c) Union (U) gate. (d) The functional module G that provides the equivalent function as two independent binary NOR and NAND functions.

TABLE II. Table of combinations for binary functions of example.

x_3x_4	x_1x_2			
	00	01	10	11
00	11	11	11	01
01	10	10	10	00
10	10	10	10	00
11	10	10	10	00

TABLE III. Table of combinations for multiplexed function $G(X_1, X_2)$ of example.

X_2	X_1			
	\emptyset	$\{f_1\}$	$\{f_2\}$	$\{f_1, f_2\}$
Φ	$\{f_1, f_2\}$	$\{f_1, f_2\}$	$\{f_1, f_2\}$	$\{f_1\}$
$\{f_1\}$	$\{f_2\}$	$\{f_2\}$	$\{f_2\}$	Φ
$\{f_2\}$	$\{f_2\}$	$\{f_2\}$	$\{f_2\}$	Φ
$\{f_1, f_2\}$	$\{f_2\}$	$\{f_2\}$	$\{f_2\}$	Φ

The multiplexed function G can be realized using SD, SG, and U gates as presented below:

$$\begin{aligned} Y &= G(X_1, X_2) \\ &= SG(\{f_1\}; X_1) USG(\{f_2\}; SD(X_2; \{f_1\})) USG(\{f_2\}; SD(X_2; \{f_2\})). \end{aligned} \quad (1)$$

The corresponding circuit configuration is depicted in Fig. 3(d).

The realization of parallel processing that can process densely multiplexed information as it is multiplexed, using the properties of wave-like information carriers without separating the information, might resolve bottlenecks of conventional binary logic circuits and might contribute to the future internet of things (IoT) and artificial intelligence (AI) society. As presented hereafter, we explore physical properties of electron spin waves as information carriers for the possible implementation of the proposed wave-parallel computing.

III. ELECTRON SPIN WAVE FOR MULTIPLEXING INFORMATION IN SEMICONDUCTORS

The electron spin wave is a spatial spin structure shown in Fig. 4(a), where the spin rotates in space by an SO-induced effective magnetic field. Because the SO interaction acts as an effective magnetic field for electrons and because it is controlled precisely through an external gate,^{60,61} the electron spin wave can be stabilized and controlled with no external magnetic field or magnetic materials. To use the electron spin wave for wave-parallel computing as discussed earlier, generation, detection, and stable transportation of an electron spin wave are fundamentally important in semiconductors. Additionally, it is necessary for parallel computing to mix and separate multiple electron spin waves and their interconversions.

To stabilize the electron spins as a wave, we suppress the spin state randomization, but we still allow the spin precessional motion for a long distance. Such a condition is realized when using a persistent spin helix (PSH) state.^{35,36} In the PSH state, the SO magnetic field is uniaxially oriented with a SU(2) spin rotation symmetry as presented

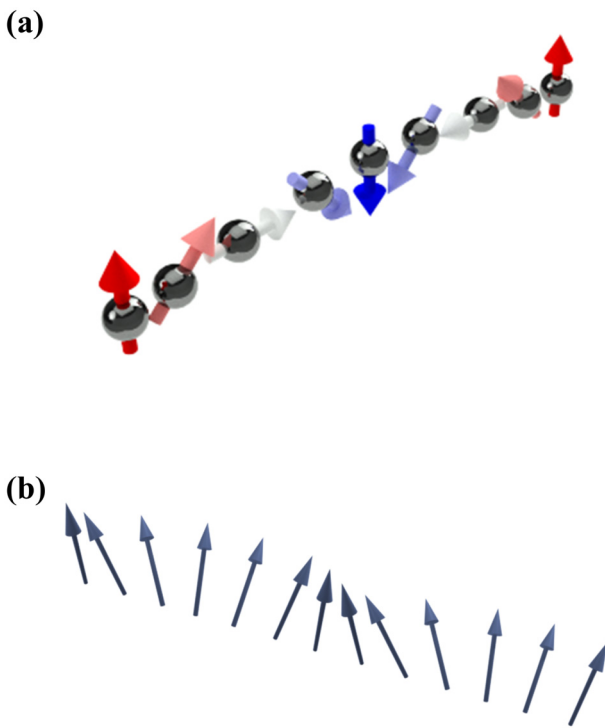


FIG. 4. Schematic illustrations of (a) electron spin wave and (b) magnetic spin wave (magnon). Electron spin moving in semiconductor forms a wave as it rotates around an effective magnetic field induced by spin-orbit interaction. Magnetic spin wave (magnon) is the corrective precessional motion of local magnetic moment in ferromagnetic and antiferromagnetic materials.

in Fig. 5(a). This symmetry is robust against both spin independent scattering and Coulomb interaction, resulting in the suppression of spin relaxation while allowing spin precession around the SO field. The induced phase of the precession becomes independent of the electron's scattering path. It is only determined by the distance the electron travels in a particular crystal orientation: the [1–10] direction in Fig. 5(a). These features make an ideal platform for stabilizing an electron spin wave.

To realize the PSH state in a (001)-oriented III-V semiconductor quantum well (QW), the strengths of two SO interactions must be mutually equal: the coefficients of Rashba (α)³² and Dresselhaus (β)³¹ SO interactions must be equal, as $|\alpha| = \beta$. The effective magnetic fields in momentum space are presented, respectively, in Figs. 5(c) and 5(d). The Dresselhaus SO interaction is material-specific, generally related to the bulk inversion asymmetry of the crystal, but it can still be controlled by the QW width and carrier density.^{62,63} Rashba SO interaction is widely tunable by the external gate electric field because it originates from the structural inversion asymmetry,^{60,61,63–66} induced by a potential gradient of the QW confinement. By switching the sign of the Rashba SO coefficient from $\alpha = \beta$ to $-\alpha = \beta$, the uniaxial SO field is rotated by 90° as shown in Figs. 5(a) and 5(b), from a PSH to an inverse (i)-PSH state.⁶⁷ Gate-controlled PSH and i-PSH states have been demonstrated in an InGaAs/InAlAs QW with a metal top gate electrode using quantum interference effect on

magnetoconductance.^{41,67,68} The possibility of switching between these two states is useful to switch the propagation of the electron spin wave. Dettwiler *et al.* showed the gate control of the Dresselhaus SO coefficient and the continuous locking of the PSH state,⁶³ corresponding to a stretching of persistent spin helices. This stretching makes it possible to modulate the wavelength of the electron spin wave by the gate. Direct determination of the α/β ratio with no fitting procedure can be achieved by measuring semiconductor narrow wires.^{68,69} Also, PSH states have been found in various materials.^{47,49–52} In a III–V semiconductor QW, the PSH state appears not only in a (001) crystal plane but also in various crystal planes, such as (110), (221), (225), and (115), with different PSH lifetimes.^{70,71} It is noteworthy that a (225)-oriented PSH state exhibits the longest lifetime among all crystal planes because the spin relaxation by cubic Dresselhaus SO field is largely suppressed.

Transferring the spin angular momentum between a photon and an electron through optical selection rules is a powerful technique for generating and detecting electron spin waves. Pioneering research exploring the direct generation of a spatially oscillating spin component has been undertaken using transient spin grating technique in GaAs/AlGaAs multiple QWs,³⁷ thereby revealing the lifetime of electron spin waves under a PSH condition by optical detection. Direct mapping of an electron spin wave in the PSH state was demonstrated in a (001)-oriented GaAs/AlGaAs QW using spatiotemporal Kerr rotation microscopy.⁴⁰ Figure 6 shows the spin polarization along the z direction at 10, 240, and 840 ps after excitation at 40 K. Although the spin polarization 10 ps after excitation is still oriented mostly along the z direction, diffusion and spin precession about the SO magnetic field develop a stripe pattern of spin up (red) and spin down (blue) electrons with a time delay [(b) 240 ps and (c) 840 ps in Fig. 6], thereby demonstrating a PSH formation. In a semiconductor wire, lateral confinement can produce an electron spin wave without the need to tune the SO coefficients because the SO field is aligned to one direction as a result of quasi-1D electron motion.^{72–74}

The drift transport of electron spin waves has been demonstrated in a gate-fitted GaAs/AlGaAs QW.⁴² Figure 7(a) shows the spatial distribution of electron spins drifting in the [1–10] and [110] directions, in addition to spin diffusion without drift motion under the PSH condition at 8 K. An electron spin wave is transported over 100 μm distance along the [1–10] direction, whereas the initial spin state is preserved along the [110] direction. Because the precession phase is only determined by the relative distance from the [1–10] direction, the electron spin wave is robust when subjected to a meandering motion shown in Fig. 7(b), which is advantageous for transport over a long distance. By applying an external magnetic field, a traveling PSH has been realized,⁴³ where the phase and group velocities are identical in an optically excited helical spin wave, thereby preserving the helical spin wave shape during the drift transport.

Although the optical method enables us to explore the fundamentals of the electron spin wave, it is limited to materials with a direct bandgap. To overcome this obstacle, fully electrical means have been established that are based on measuring quantum corrections to the conductivity to obtain the lifetime of electron spin waves in the vicinity of the PSH state.⁷⁵ This finding is expected to pave the way for exploring electron spin waves in various bandgap materials from semiconductors to metals.

The ultimate goal associated with electron spin waves is to process multiple information in parallel, as described earlier. A step

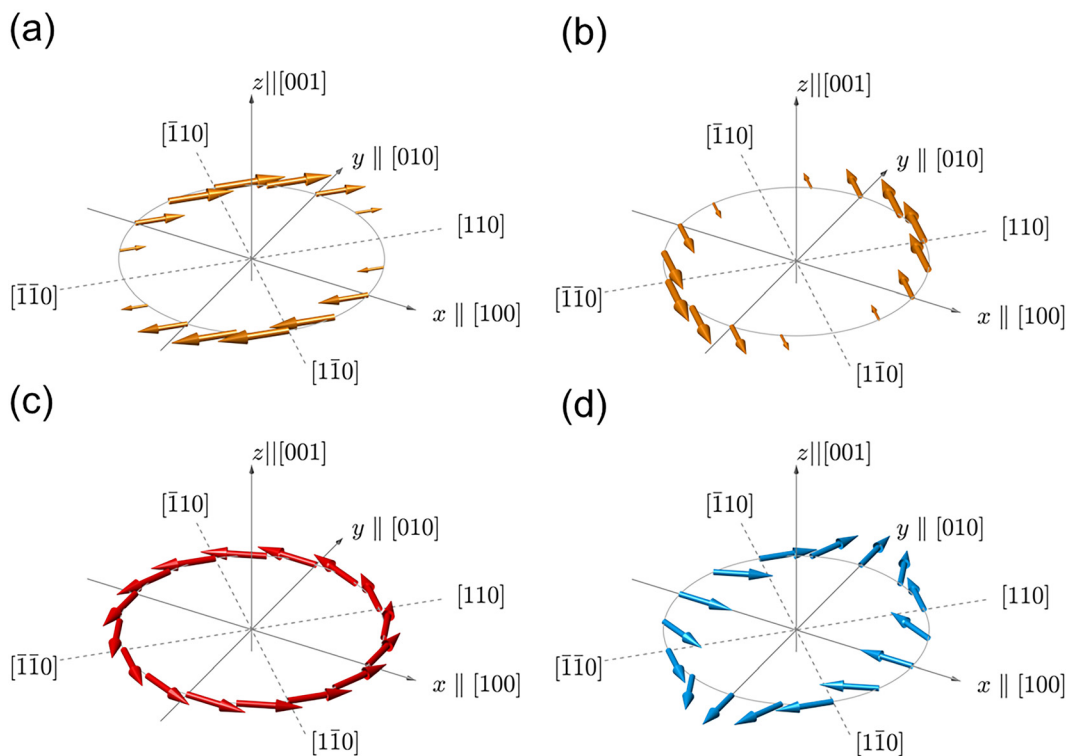


FIG. 5. Spin-orbit induced effective magnetic field vectors for (a) persistent spin helix condition ($\alpha = \beta$), (b) inverse (i)-persistent spin helix condition ($-\alpha = \beta$), (c) Rashba and (d) linear Dresselhaus contributions in a (001)-oriented III-V semiconductor quantum well reprinted.³⁸ System parameters are g factor < 0 , Rashba spin-orbit coefficient $\alpha > 0$ [except for (b), where $\alpha < 0$], bulk Dresselhaus spin-orbit value $\gamma < 0$, linear Dresselhaus spin-orbit coefficient $\beta_1 > 0$. Reproduced with permission from M. Kohda and G. Salis, *Semicond. Sci. Technol.* **32**, 073002 (2017). Copyright 2017 Institute of Physics.

18 November 2023 08:23:47

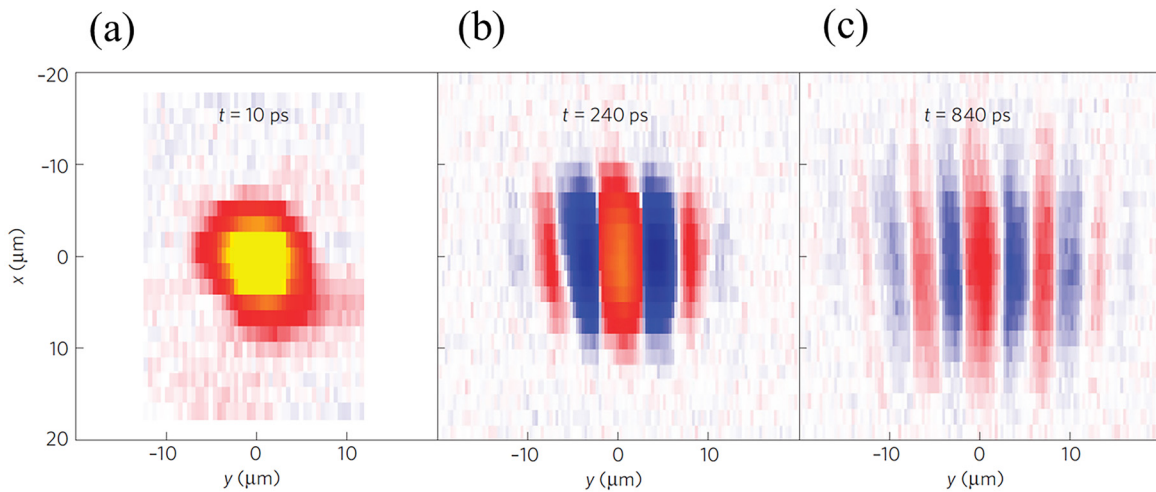


FIG. 6. Spatial evolution of the z-component of the spin polarization measured by spatiotemporal Kerr rotation at (a) 10, (b) 240, and (c) 840 ps after the excitation in a 12 nm GaAs/AlGaAs QW obtained from an earlier report.⁴⁰ The doping profile of the QW is designed such that the Rashba SO interaction nearly balances the Dresselhaus SO interaction. Measurement temperature is at 40 K. Reproduced with permission from Walser *et al.*, *Nat. Phys.* **8**, 757–762 (2012). Copyright 2012 Springer Nature.

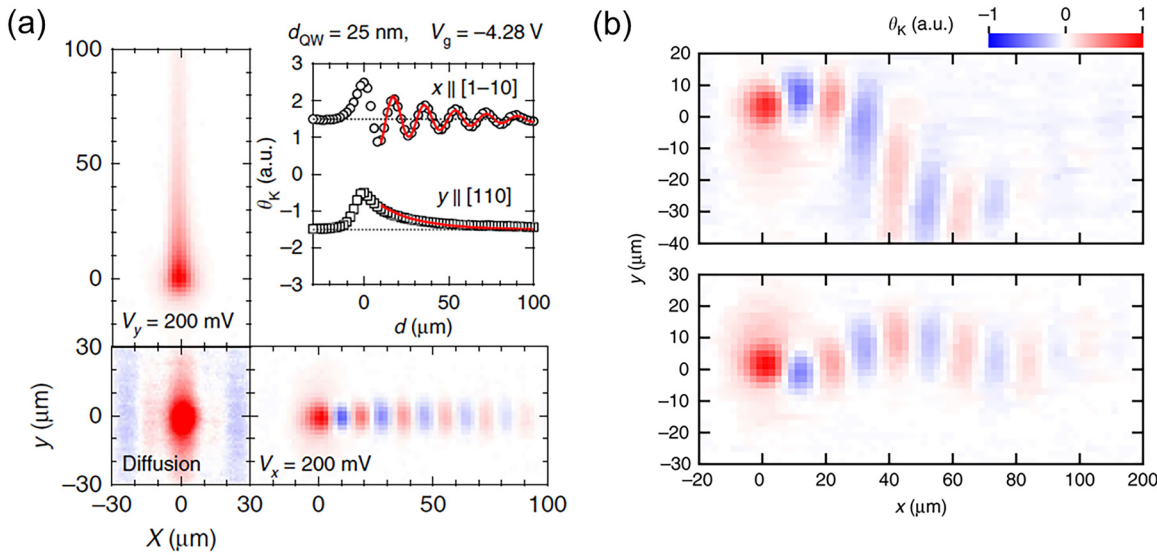


FIG. 7. (a) Spatial distribution of electron spins drifting along the $[1-10] \parallel x$ and $[110] \parallel y$ directions with helical and homogeneous spin textures, respectively, and spin diffusion without drift motion of a PSH state in a GaAs/AlGaAs quantum well with applied gate voltage V_g from an earlier report.⁴² Measurement temperature is at 8 K (b) Drift spin transport driven by DC bias voltage ($V_x^{dc} = 100$ mV) along x direction with sinusoidal voltage ($V_y^{ac} = 200$ mV) applied in y direction to modulate orbital trajectory. Upper and lower panels correspond to the different frequency of the V_y^{ac} adjusted to the repetition rate of pulsed laser 82.46 MHz and twice the frequency. Adapted from Kunihashi *et al.*, Nat. Commun. 7, 10722, (2016). Copyright 2016 Author(s), licensed under a Creative Commons Attribution (CC BY) license.

toward multiplexing the information is to mix and separate electron spin waves in semiconductors. From a theoretical perspective, the PSH state naturally holds the multiple electron spin waves.⁷⁶⁻⁷⁸ Figure 8(a) presents dispersion of the eigenmodes of the spin diffusion equation, i.e., the spin decay rate of electron spin waves as a function of normalized wave number q_y/q_0 .⁷⁸ Local minima for the decay rate correspond to the two helical and one homogeneous spin modes at $q_y/q_0 = \pm 1$ and $q_0 = 0$.⁷⁸ The minimum decay rates at $q_y/q_0 = \pm 1$ correspond to the PSH condition. The helical spin mode is characterized by a finite wave number $q_0 = \pm 2m^*(|\alpha| + \beta)/\hbar^2$, where m^* denotes the effective mass and where \hbar is the reduced Planck's constant. Because the direction of the uniaxial SO field depends on the relative sign of α and β , actually the PSH and i-PSH states shown, respectively, in Figs. 5(a) and 5(b), the helical spin mode propagates along the $[1-10]$ direction for $\alpha = \beta$ and along the $[110]$ direction for $-\alpha = \beta$. Figure 8(b) presents the helical spin mode propagating along the $[1-10]$ direction under the PSH condition. In such a condition, the homogeneous spin mode at $q_0 = 0$ corresponds to a spatially homogeneous spin orientation along the $[110]$ axis [Fig. 8(c)]. The spin relaxation rate for a non-spatial spin texture, the D'yakonov-Perel' (DP) spin relaxation rate, is also plotted as a dotted line in Fig. 8(a), with a value that is one order of magnitude larger than that of the PSH state. Electron spin waves with wavelengths close to the PSH state are also stable. They can be used to multiplex electron spin waves with various wavelengths. To check this point, we conducted Monte Carlo (MC) simulations for two electron spin waves with different wavelengths close to the PSH state. Parameters for the Rashba coefficient, linear and cubic Dresselhaus coefficients, spin diffusion constant, and carrier density are, respectively, -1.75×10^{-13} eV m, 1.70×10^{-13} eV m, 0.46×10^{-13} eV m, $0.13 \text{ m}^2/\text{Vs}$, and $3.2 \times 10^{15} \text{ m}^{-2}$. Figure 9(a)

shows the initial two spin waves with $q = 0.8q_0$ and $1.2q_0$, where $q_0 = 0.53 \mu\text{m}^{-1}$ excited at $t = 0.0$ ns and their spatiotemporal variation in a $1.0 \mu\text{m}$ -width wire. The interference of the two electron spin waves with different wavelengths generates complex waveforms both in the spatial and time domains. Figure 9(b) exhibits the time-space map, where the initial wave pattern is preserved while the amplitude decays. To resolve the time evolution of each wave, we take fast Fourier transforms of the data shown in Fig. 9(b) and plot the time evolutions of spin modes in Fig. 9(c). Two helical modes are observed clearly at the distinguished wave numbers. They decay on similar time scales, indicating the stable preservation of multiple electron spin waves. This stable decay constitutes the basis for multiplexing information by electron spin waves.

The separation of a specific mode among multiplexed electron spin waves is implemented further. This implementation corresponds to the SD gate operation in wave-parallel computing. In MC simulation, we first excite three electron spin waves with different wave numbers of $q = 0.6q_0$, $1.0q_0$, and $1.4q_0$. Then, we simulate their spatiotemporal evolution in Fig. 10(a). Whereas the multiplexed electron spin waves form a complex wave pattern at the initial condition [$t = 0.0$ ns in Fig. 10(a)], a single electron spin wave remains after some time evolution [$t = 0.9$ ns in Fig. 10(a)]. Because the spin decay rate of electron spin waves increases with q^2 , as presented in Fig. 8(a), the wave number $q_y/q_0 = \pm 1$ at PSH condition preserves the electron spin wave, but other wave numbers $q \neq |q_0|$ decay and vanish, as presented in Fig. 10(b). The time evolution of spin modes in Fig. 10(c) clearly illustrates the different decays for three spin modes. Any electron spin wavelength can be selected by tuning the SO effective field through the gate,⁶¹ selecting a desired electron spin wave from the initial multiple inputs. This selection corresponds to the electron spin

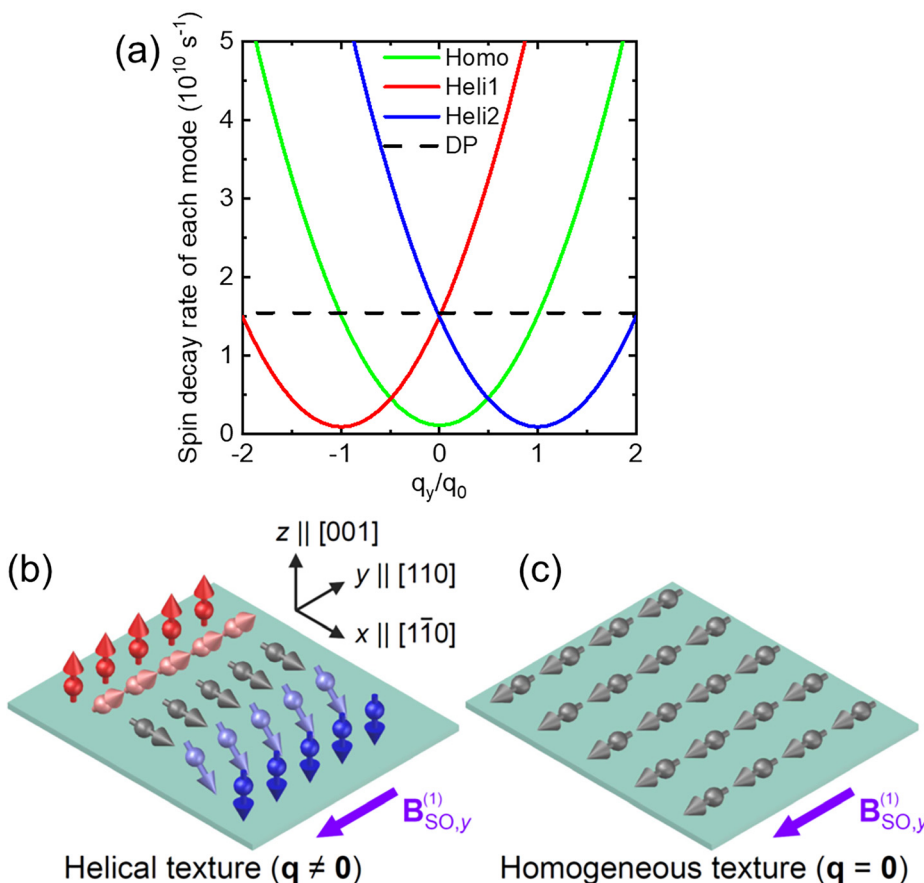


FIG. 8. (a) Dispersion relation of the eigenmodes of the spin-diffusion equation for wave number $q_x = 0$. The vertical axis corresponds to the spin decay rate of electron spin waves. The minimum decay rates of two helical and one homogeneous modes are at $q_y/q_0 = \pm 1$ and 0, respectively. The PSH state corresponds to $q_y/q_0 = \pm 1$. Schematic view of (b) helical and (c) homogeneous spin textures. Adapted from Saito *et al.*, Phys. Rev. Res. **4**, 043217 (2022). Copyright 2022 Author(s), licensed under a Creative Commons Attribution (CC BY) license.

wave filter.⁷⁹ In both multiplexing and filtering electron spin waves, a key is control of the spin diffusion constant in the spin wave dispersion [Fig. 8(a)] because the spin diffusion constant determines the curvature of q^2 dependence.

IV. SPIN WAVE-BASED MULTI-STATE STORAGE FOR INFORMATION MULTIPLEXING

If information is multiplexed based on the combination of whether a certain state exists or not, as presented in Fig. 2(b), then, a corresponding storage technique, allowing the storage of information directly as a “state” is unavoidable. Such a storage concept in which a particular state is read or written selectively might be achieved by exploiting magnetic spin waves (magnons).⁷⁹ Hereafter, the magnetic spin wave is designated simply as a spin wave if it is not distinguished from an electron spin wave. Later, we introduce spin waves that are useful not only for data processing¹⁵ but also as a tool for selective data writing. In addition, we discuss the perspective that spin wave-assisted data writing can realize multi-state storage for information multiplexing by virtue of the selective switching characteristics.

A magnet having spontaneous magnetization is exploited as a medium of data storage. For example, the upward and downward magnetized states of a perpendicular magnet can be regarded, respectively, as information of “1” and “0.” Hard-disk drives and MRAM are well known as representative data storage using nanometer-scale magnets.

Growing demand for ultrahigh density and low power-consumption storage, as driven by demands for cloud computing systems and various devices, has reduced the size of information bits considerably. To achieve thermally stable data storage in such magnets at reduced size, a high magnetic anisotropy (K) material is unavoidable because the thermal stability factor is proportional to the product of K and the magnetic volume. At the same time, a highly efficient means for data writing, i.e., magnetization switching, is needed. The external energy-assisted switching techniques, such as heat-assisted⁸⁰ and microwave-assisted means,⁸¹ are promising to fulfill the requirements of both high thermal stability and low energy switching simultaneously. Apart from those external energy-assisted means, spin waves are useful to reduce the switching fields of magnets. This concept, which is known as “spin wave-assisted switching,” has been proposed and demonstrated experimentally.^{82–85} As shown in Table I, the magnetic spin wave and the electron spin wave exhibit similar characteristics. Consequently, one might anticipate that those can be converted through transfer of the spin angular momentum,⁸⁶ producing an element for multiplexed information storage through spin waves.

Figure 11(a) shows the concept of spin wave-assisted switching in an exchanged-coupled bilayer with hard and soft magnetic layers. The hard magnetic layer with high K acts as a data storage layer, whereas the soft magnetic layer acts as a medium for spin wave dynamics. For switching, a static magnetic field (H) and an rf magnetic field (h_{rf}) are

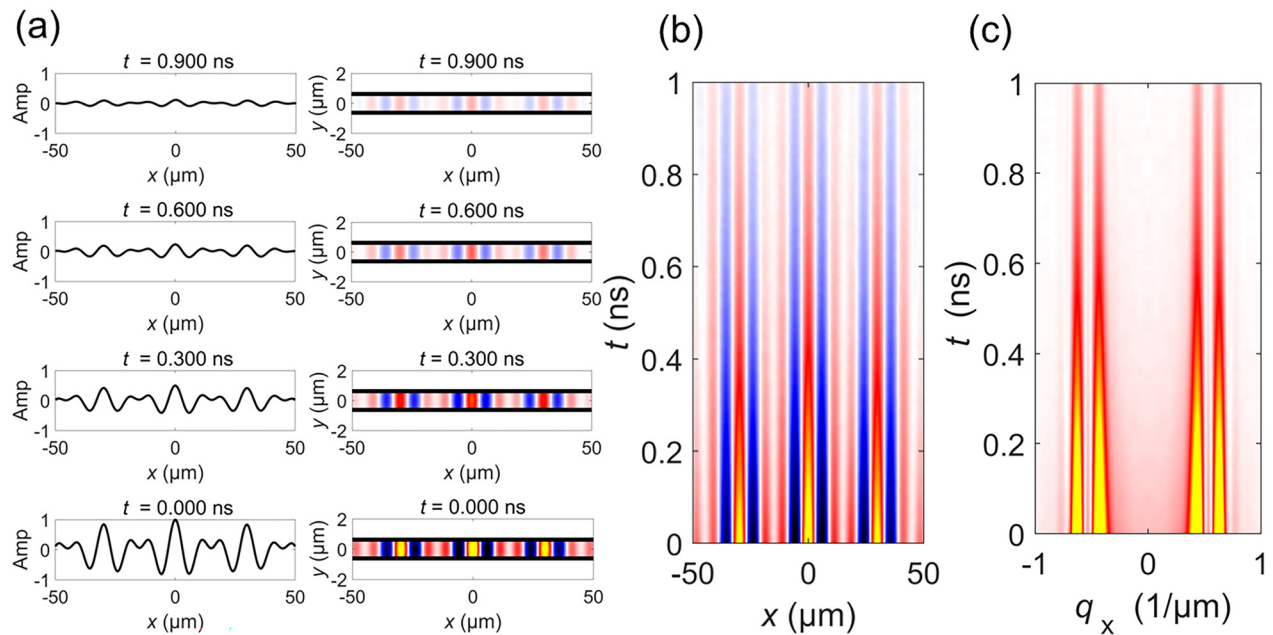


FIG. 9. Monte Carlo based spin dynamics simulation in a $1.0 \mu\text{m}$ -width wire structure for two electron spin wave excitations with $q = 0.8q_0$ and $1.2q_0$ ($q_0 = 0.53 \mu\text{m}^{-1}$), both of which are close to the PSH state: (a) spatial spin wave patterns at various times after the initial excitation, (b) time-space mapping of spatial spin wave pattern, and (c) time evolution of spin modes.

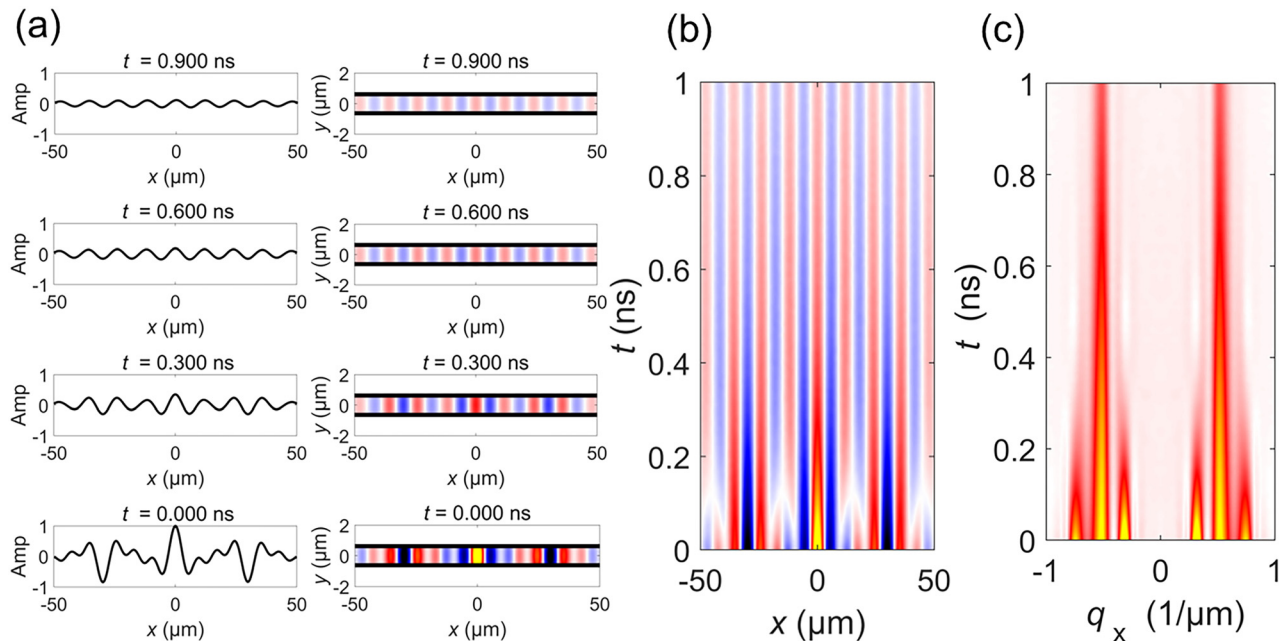


FIG. 10. Monte Carlo based spin dynamics simulation to demonstrate the electron spin wave filter. Three electron spin waves with different wavelengths of $q = 0.6q_0$, $1.0q_0$, and $1.4q_0$ ($q_0 = 0.53 \mu\text{m}^{-1}$) are excited in a $1.0 \mu\text{m}$ -width wire structure. The PSH condition is fulfilled at $q = 1.0q_0$. (a) Spatial spin wave patterns at various times after the initial excitation. Three electron spin waves are excited at $t = 0.0 \text{ ns}$. Following the decay of two electron spin waves, only the specific electron spin wave remained after $t = 0.9 \text{ ns}$. (b) Time-space mapping of spatial spin wave pattern. (c) Time evolution of spin modes.

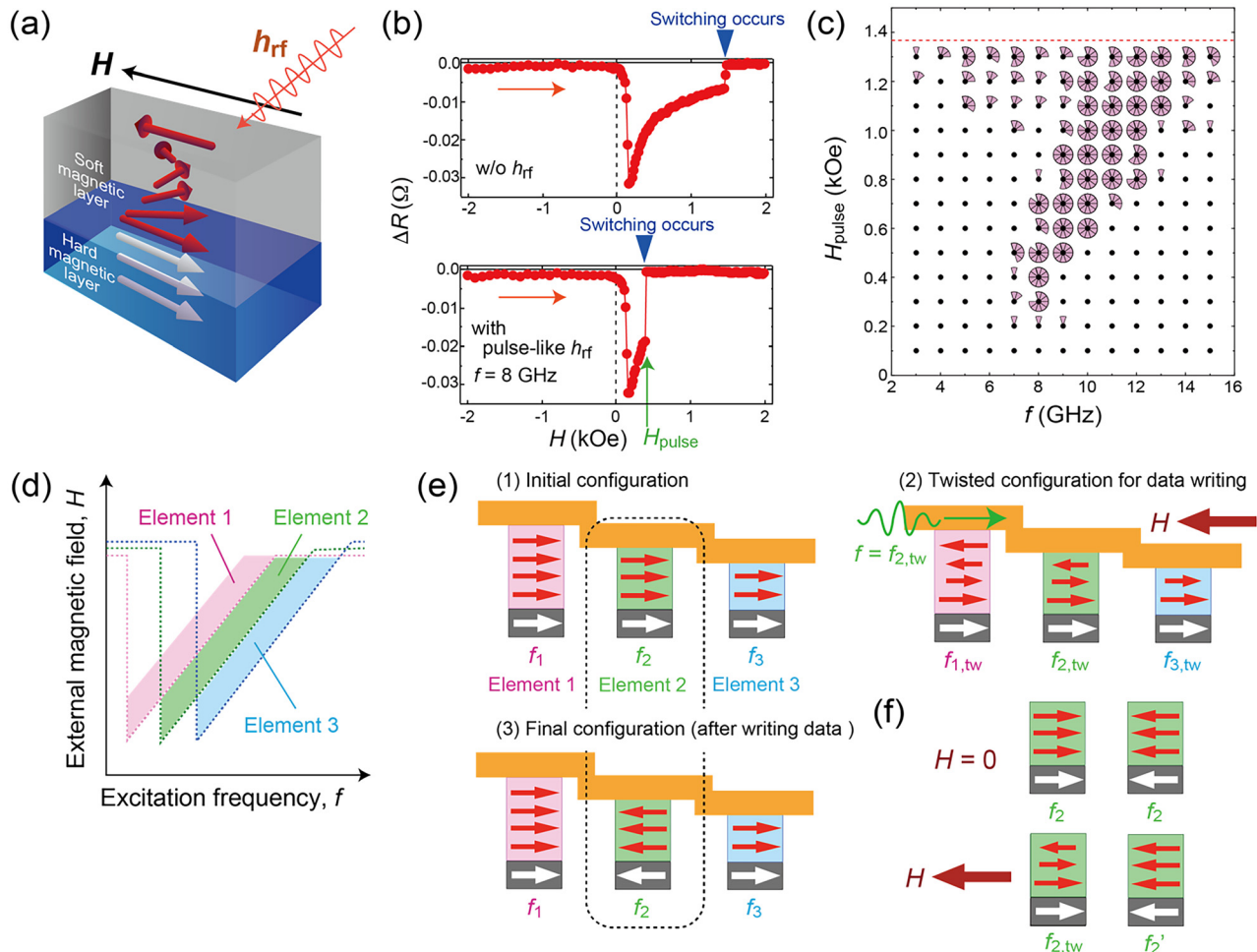


FIG. 11. (a) Concept of spin wave-assisted switching in an exchanged-coupled bilayer with hard and soft magnetic layers. A static magnetic field (H) and an rf magnetic field (h_{rf}) are applied to excite the spin wave in the soft magnetic layer, leading to reduction in the switching field (H_{sw}) of the hard layer via exchange coupling. (b) Magnetoresistance curves ($\Delta R-H$ curves) measured without h_{rf} and with a pulse-like h_{rf} of 8 GHz applied at 0.4 kOe.⁸⁵ (c) Experimentally mapped switching events of the $L1_0$ -FePt layer in the $H-f$ plane. The h_{rf} of 97 Oe was applied to the element. For each parameter in the plane, ten measurements were taken. The number of switching events is represented by the number of sectors. The red dashed line represents H_{sw} without h_{rf} application.⁸⁵ (d) Schematic illustration of switching event map for selective switching in three storage elements with different soft magnetic layer thicknesses. Each hatched area corresponds to the switching condition for each element (elements 1, 2, and 3). (e) Data writing process for multi-state data storage elements. Three data storage elements are aligned and connected with a channel of electron spin wave, and show the initial configuration, twisted configuration, and final configuration. (f) Illustration showing that application of an external magnetic field leads to the difference in the total energy between a switched element and non-switched elements, i.e., $f_{2,tw} \neq f'_2$. This is a basic concept for detection of whether the state exists or not. Reproduced with permission from Zhou *et al.*, Appl. Phys. Lett. **110**, 082401 (2017). Copyright 2017 AIP Publishing LLC.

applied to the bilayer element similarly to microwave-assisted switching (MAS) using a single hard magnetic layer.⁸² For spin wave-assisted switching, however, h_{rf} excites the spin wave modes in the soft magnetic layer, thereby leading to reduction in the switching field (H_{sw}) of the hard layer via exchange coupling through the interface separating the hard and soft magnetic layers.

An example of spin wave-assisted H_{sw} reduction⁸⁵ is presented in Fig. 11(b), which was done for the in-plane magnetized bilayer consisting of a 10 nm-thick $L1_0$ -FePt hard magnetic layer and a 100 nm-thick $Ni_{81}Fe_{19}$ soft magnetic layer. The spin wave assistance was examined by ascertaining whether the switching event occurs, or not, after

applying the pulse-like h_{rf} with a certain frequency (f) at a magnetic field (H_{pulse}). The magnetoresistance curves show the resistance change (ΔR) depending on the magnetic structure of the bilayer, indicating that magnetization switching occurs at $H = 1.37$ kOe in the case without h_{rf} . However, if the pulse-like h_{rf} with $f = 8$ GHz is applied at $H_{pulse} = 0.4$ kOe, then switching can be induced even at $H = 0.4$ kOe. Figure 11(c) displays the experimentally mapped switching events of the FePt layer in the $H-f$ plane. If f and H_{pulse} satisfy the switching conditions, then, the H_{pulse} corresponds to H_{sw} with one sector added to represent the switching event in the $H-f$ plane. As might be readily apparent, H_{sw} is decreased from $H_{sw} = 1.37$ kOe for the case without

h_{rf} application by application of $h_{rf} = 97$ Oe. The most remarkable H_{sw} reduction is observed at $f = 8$ GHz, at which switching occurs even at $H_{pulse} = 0.2$ kOe, representing the H_{sw} reduction from 1.37 to 0.2 kOe.

Another important feature that is apparent in Fig. 11(c) is that the switching events exist in a limited region of the H - f plane. Numerical simulation indicated that the experimentally observed switching condition of H_{pulse} and f is determined by the dispersion relation of perpendicular standing spin wave (PSSW) modes (not shown, but available in an earlier report⁸⁵) In other words, switching events do not occur when the PSSW is not excited. This characteristic is completely different from that of MAS.⁸¹ Spin wave-assisted switching occurs through the resonant excitation process of spin wave modes. A map of the switching conditions presented as Fig. 11(c) indicates that spin wave-assisted switching can serve as selective switching. If multiple storage elements with different soft magnetic layer thicknesses can be prepared, e.g., the three elements (elements 1, 2, and 3) as illustrated in Fig. 11(e), which possess different switching conditions of H and f because the resonant frequency of PSSW changes depending on the layer thickness, then the selective switching of one element is possible by proper selection of H and h_{rf} as schematically shown in Fig. 11(d). This feature is advantageous also for multi-state storage requiring selective data writing. It should also be noted that no transistor for memory cell selection is required because of the selective data writing. The study introduced above was based on experiments done using the “in-plane” magnetized bilayer element. As in the case of in-plane system, the spin wave-assisted H_{sw} reduction can be achieved also for the “perpendicularly” magnetized bilayer element^{87,88} using a circular nanodot of an exchange-coupled bilayer with $\text{Ni}_{81}\text{Fe}_{19}$ having a magnetic vortex and a perpendicularly magnetized $L1_0\text{-FePt}$.

Considering the selective switching characteristics of spin-wave assistance and the H_{sw} reduction, this switching technique has potential for the multi-state data storage for wave-parallel computing.⁷⁹ Figure 11(e) is an illustration explaining a data writing process for multi-state data storage elements. Three data storage elements are aligned and connected with a common channel of electron spin waves. At the “initial configuration,” the resonance frequencies for Elements 1, 2, and 3 are, respectively, f_1 , f_2 , and f_3 . The application of external magnetic field in the opposite direction to the magnetizations, which is less than the switching fields for all the elements, engenders the “twisted configuration” with the resonance frequencies of $f_{1,tw}$, $f_{2,tw}$, and $f_{3,tw}$. If the electron spin wave can excite the spin wave dynamics only for Element 2 because of the wave with frequency $f = f_{2,tw}$, then the switching event occurs only for Element 2. Then, the final configuration of data storage elements is obtained as shown in (3) of Fig. 11(e). Additionally, we might detect whether the state exists or not through the magnetic resonance techniques. As depicted in Fig. 11(f), the application of H enables us to distinguish whether Element 2 has been switched or not because $f_{2,tw} \neq f'_2$, where f'_2 is the resonant frequency for parallel configuration of hard and soft magnetic layers under the application of H . If we measure the magnetic resonance spectra for the initial configuration and the final configuration of Fig. 11(e), then the resonance peaks appear at $f_{1,tw}$, $f_{2,tw}$, and $f_{3,tw}$ for the initial configuration, and at $f_{1,tw}$, f'_2 , and $f_{3,tw}$ for the final configuration. This spectral measurement corresponds to the detection of whether the state exists or not, corresponding to the multi-state storage. Of course, many technical issues remain to be resolved. A crucially important issue is how to transfer the data carried by electron spin waves in the channel to the bilayer element.

One possible way is to exploit the spin transfer torque acting on the magnetization of the soft magnetic layer from the electron spin wave. To realize this concept, further investigation must be undertaken for the fundamental spin transport phenomena in ferromagnet/semiconductor hybrid structures, as discussed next.

V. FERROMAGNET/SEMICONDUCTOR HYBRID STRUCTURE FOR GENERATING AND CONTROLLING ELECTRON SPIN WAVE AND MAGNETIC SPIN WAVE (MAGNON)

Highly spin-polarized ferromagnetic materials and their use to spin injection in semiconductors are indispensable for efficiently creating spin waves in semiconductors and/or storing multiple data of spin waves into ferromagnetic layers. Pioneering works toward high spin injection efficiencies have studied paramagnetic semiconductor ZnMnSe with spin injection efficiency of 86% at 3 T.⁸⁹ By employing CoFe/epitaxial MgO tunnel barrier structure where the coherent tunneling is expected through Δ_1 band, 47% of spin injection efficiency has been demonstrated.⁹⁰ Regarding ferromagnetic semiconductor/nonmagnetic semiconductor hybrid structures, namely, a $(\text{Ga},\text{Mn})\text{As}/n\text{-GaAs}$ Esaki diode, a spin injection efficiency into GaAs of 70%–85% was detected by spin-LED^{91,92} and spin-valve^{93,94} structures, which exhibit efficient spin injection without an external magnetic field. This is because $(\text{Ga},\text{Mn})\text{As}$ is of half-metallic nature where the only majority spin is occupied at the Fermi level (E_F) in the density of state. Thanks to this high spin injection efficiency, Eberle *et al.* demonstrated coherent spin rotation in gate-controlled spin FET based on a $(\text{Ga},\text{Mn})\text{As}/n\text{-GaAs}$ spin Esaki diode,⁹⁵ which is a promising step toward the generation of electron spin waves by electrical means.

Co-based Heusler alloy (Co_2YZ , where Y is usually a transition metal and Z is a main group element) is also a promising candidate for use as a highly polarized spin source because many Co-based Heusler alloys, such as Co_2MnSi (CMS) and Co_2MnGe (CMG), have theoretically 100% spin polarization at E_F because of their half-metallic nature^{96–99} and high Curie temperatures that are well above room temperature (RT).¹⁰⁰ Several reports have described studies of spin injection through optical detection in spin LEDs with a Co-based Heusler alloy electrode, such as CMG,¹⁰¹ $\text{Co}_{2.4}\text{Mn}_{1.6}\text{Ga}$,¹⁰² or Co_2FeSi (CFS),¹⁰³ and through electrical detection in lateral spin-transport devices with CFS^{104,105} or $\text{Co}_2\text{FeAl}_{0.5}\text{Si}_{0.5}$ (Ref. 106). In particular, Peterson *et al.* observed nonlocal spin signals up to RT by using CFS electrodes with its injection efficiency of 30% at 20 K.¹⁰⁵

To control the electron spin wave, spin injection into a semiconductor two-dimensional electron gas (2DEG), where the Rashba SO interaction is modulated by the gate, is also prerequisite.^{95,107,108} Here, we describe the demonstration of highly efficient spin injection into a GaAs channel¹⁰⁹ and an AlGaAs/GaAs 2DEG channel¹¹⁰ up to RT from a half-metallic CMS spin source. Figures 12(a) and 12(b), respectively, show a schematic of lateral spin injection device with a layer structure of CMS (5 nm)/CoFe (1.3 nm)/GaAs (001) and its scanning transmission electron microscope image.¹⁰⁹ An atomically flat and abrupt interface facing GaAs was formed. Figure 12(c) shows a non-local voltage V_{NL} as a function of in-plane magnetic field at 4.2 K. A clear spin-valve signal was observed: V_{NL} changes because of switching between the parallel (P) and antiparallel (AP) states for the relative magnetization configurations between the injector and detector contacts. Figure 12(d) presents V_{NL} as a function of out-plane magnetic field H_z . The V_{NL} for the P (AP) configuration increased (decreased)

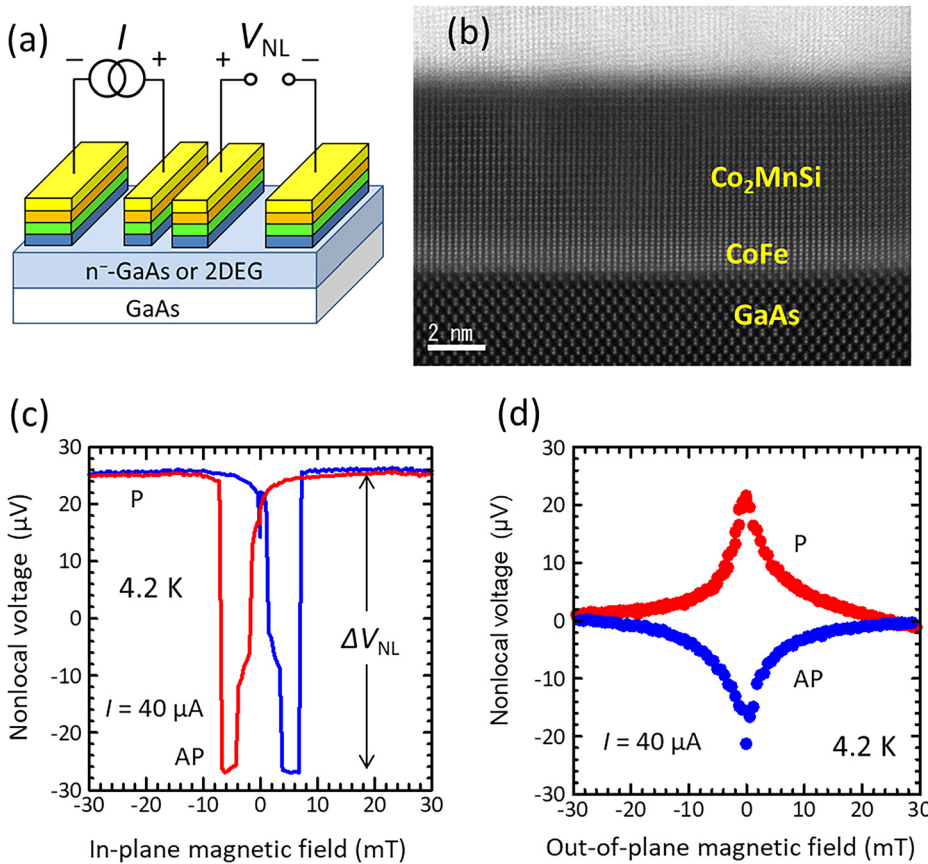


FIG. 12. (a) Schematic diagram of a lateral spin-transport device with a non-local geometry. (b) HAADF STEM image of a layer structure of Ru/Co₂MnSi/CoFe(1.3 nm)/GaAs(001). (c) Typical spin-valve signal and (d) Hanle signals for a Co₂MnSi/CoFe/n-GaAs junction at 4.2 K from an earlier report.¹⁰⁸ Reproduced with permission from Ebina et al., Appl. Phys. Lett. **104**, 172405 (2014). Copyright 2014 AIP Publishing LLC.

gradually as $|H_z|$ increased. This change is ascribed to the Hanle effect: the spins injected in the GaAs channel dephase because of the precession by H_z , resulting in decreased spin accumulation in the GaAs channel. The observation of both the spin-valve signal and the Hanle signals provides the most rigorous evidence of injection, transport, and detection of spin-polarized electrons in the CMS/CoFe/n-GaAs lateral transport device. The estimated spin polarization was 52%, a value almost 13 times larger than that for the CoFe/n-GaAs sample.¹¹¹

We also describe spin injection into an AlGaAs/GaAs-based 2DEG channel with high mobility, which is a platform to generate and control the electron spin wave. We observed a non-local spin-valve signal at T from 4.2 K to RT in a spin injection device with an AlGaAs/GaAs 2DEG channel and a CMS spin source.¹¹⁰ The spin-valve signal shows no monotonic decrease concomitantly with increasing T . The signal reaches the maximum intensity at about 80 K. This finding contrasts with the result observed for bulk GaAs, in which a monotonic decrease in spin-valve signals with increasing T was observed.^{100,109} Moreover, the spin-valve signal decreased by a factor of about 5.6 with increasing T from 4.2 to 294 K. This factor is smaller than those values reported in bulk GaAs devices. This result suggests that the spin-valve signal in a 2DEG channel is less sensitive to temperature than that in a bulk GaAs, which is promising for realizing future spin-based wave-parallel computing systems that can operate at higher temperatures.

We briefly describe the effect of domain structures formed in the ferromagnet on the spin injection efficiency. Typical size of domain

walls (DWs) for a thin film of Co-based Heusler alloy is in the order of a few hundreds of nanometers, which is comparable to those of conventional 3d-transition metals, such as Fe or CoFe. Since we prepared wire-shaped CMS electrodes with width of 0.5 μm and length of 10 μm to enhance the shape anisotropy in the spin injection devices, the influence of domain structures is almost negligible. However, if the size is increased, multiple domains are randomly introduced in the injection electrode, resulting that the spin injection efficiency is reduced due to the randomly oriented spin polarization.

VI. INTERCONVERSION AMONG LIGHT, ELECTRON SPIN WAVE, AND MAGNETIC SPIN WAVE (MAGNON)

Interconversion of light helicity, electron spin waves, and magnetic spin waves (magnons) is crucial to share the wave-based information in communication, processing, and storage. A basic principle for such interconversion is the transfer of spin angular momentum in each information carrier through optical selection rule,⁵³ spin pumping,^{112–114} spin absorption,^{115,116} and spin transfer torque.^{117,118}

As we have discussed in Sec. III, optical selection rule is the basic principle for opto-electric interconversion between the light helicity and the electron spin wave.⁴⁰ A Gaussian beam with circular polarization has been used to generate a spatially uniform spin polarization as an initial state. Then, spin-polarized electrons excited are diffused away from the excited position. As shown in Fig. 13, spatial spin precession takes place around the uniaxial SO fields due to PSH state,

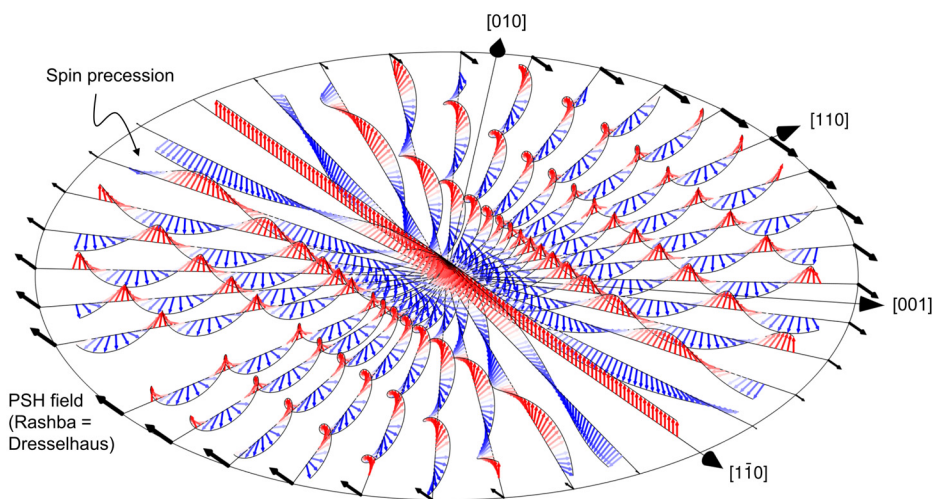


FIG. 13. Schematic illustration for rotational spin motion when electron spins spread out from the center. Because of the uniaxial SO field due to PSH state, rotational motion of electron spins forms an electron spin wave.

resulting in the formation of an electron spin wave whose wavelength is determined by the strength of the SO field. Based on this diffusive spin motion, right and left circular polarization in the Gaussian beam, namely, the helicity of light, is converted to the phase of the electron spin wave. As schematically shown in Fig. 14(a), Gaussian beam excitation with right circularly polarized (σ^+) light is converted to the positive electron spin wave where the polarization of maximum amplitude is spin up (s^+) after the spin diffusion. On the other hand, the excitation with left circularly polarized (σ^-) light generates the opposite phase of the electron spin wave, meaning that the polarization of maximum amplitude is spin down (s^-). As a result, the helicity of light as information carriers is imprinted to the phase of the electron spin wave. Such π -phase control of the electron spin wave becomes crucial for the majority gate operation.¹¹⁹ Since the majority gate employs constructive or destructive interference of electron spin waves, the inputs of electron spin waves should be either same phase or π -phase difference controlled by the helicity of light.

The ultimate goal associated with electron spin waves is to process multiple information in parallel. This requires the generation of multiplexed electron spin waves through opto-electric interconversion. To this end, we further require the spatial modulation of light helicity to directly generate electron spin waves with arbitrary shape and wavelength. As schematically shown in Fig. 14(b), the helicity of light is modulated alternately between right (σ^+) and left (σ^-) circular polarization within the Gaussian beam spot. Such a periodic modulation of σ^+ and σ^- polarization is directly converted to the electron spin wave through optical selection rule. Spatial light modulators allow continuously variable phase modulation of light in each separate pixel, controlling the polarization and light intensity within the Gaussian beam spot.^{120,121} This enables us to realize the electron spin wave of arbitrary shape and wavelength, being advantage for multiplexed electron spin waves. As a first step toward this goal, optical vortices are examined for the realization of spatially modulated light helicity and its conversion to the electron spin polarization.¹²² As shown in Figs. 15(a) and 15(b),

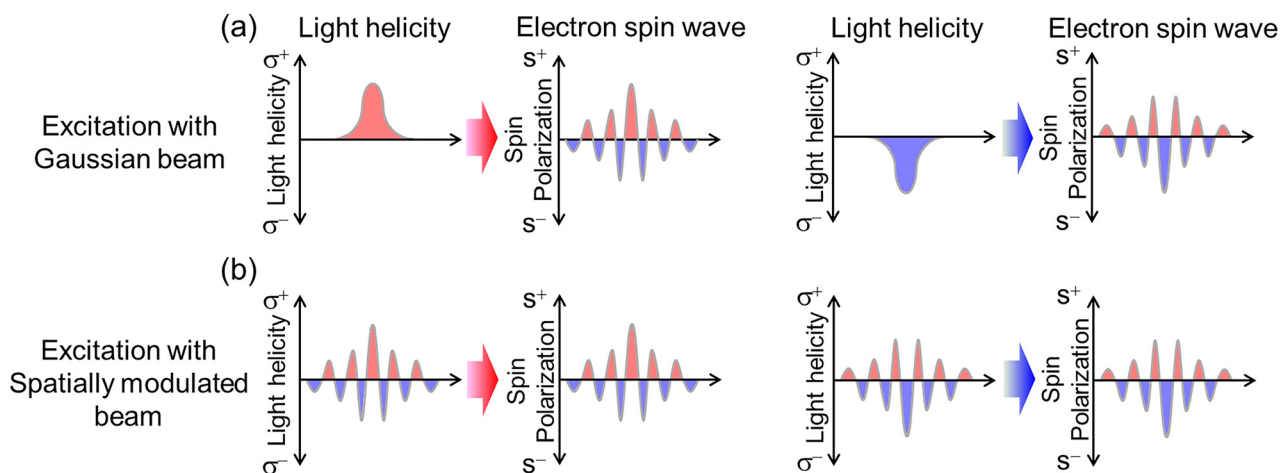


FIG. 14. Interconversion from light to electron spin wave. (a) Gaussian beam excitation with right/left circularly polarized (σ^+/σ^-) light converted to the electron spin wave with positive/negative phase. (b) Spatially modulated light helicity converted to the electron spin wave. The helicity of light is modulated alternately between right (σ^+) and left (σ^-) circular polarization within Gaussian beam, which directly reflects to the phase of electron spin wave.

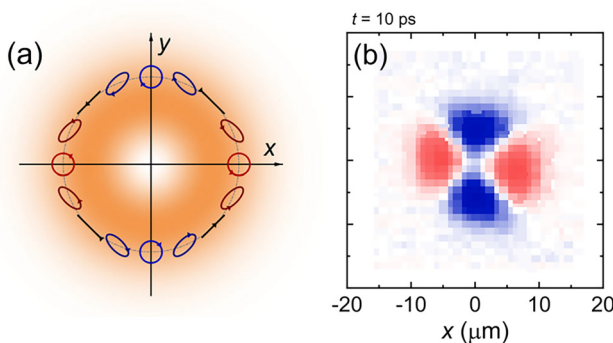


FIG. 15. Imprinting of (a) vector vortex beam with a spatial modulation of light helicity to (b) the spatial pattern of electron spin polarization probed by the Kerr rotation in a GaAs/AlGaAs QW structure. The Kerr rotation map is taken after 10 ps excited by a vector vortex beam with spin and orbital angular momentum (s, l) = (1, 1). Reproduced with permission from Ishihara *et al.*, Phys. Rev. Lett. **130**, 126701 (2023). Copyright 2012 Springer Nature.

the vector vortex beam with a spatial modulation of light helicity [Fig. 15(a)] has been imprinted to the spatial pattern of electron spin polarization in a GaAs/AlGaAs QW structure. Figure 15(b) exhibits the Kerr rotation map after 10 ps excited by a vector vortex beam with spin and orbital angular momentum (s, l) = (1, 1). Since spatial patterns of light are considered as information carrier,¹²⁰ interconversion of various spatial structures between light helicity and electron spin waves would be the key to implement the wave-parallel computing architecture.

We also describe the electrical generation of electron spin waves by using spin injection through ferromagnet/semiconductor hybrid structures. Similar to the photo-excited spin polarization, the electrical spin injection from a single domain ferromagnet to a semiconductor QW generates spatially uniform spin polarization as an initial state.^{107,110} Then, injected spin polarized electrons start to rotate around the SO field with drift and/or diffusion under an applied electric field,^{95,108} resulting in the formation of electron spin waves. In order to realize coherent spin rotation, the size of the ferromagnet electrode should be smaller than the wavelength of the electron spin wave.¹¹⁰ The phase of the electron spin wave can be controlled by either the polarity of current through the ferromagnet/semiconductor interface or the magnetization direction of the ferromagnet.¹¹⁰

In ferromagnetic materials, magnetic moments form various spatial structures as a stationary state. For example, Néel/Bloch domain walls and Skyrmions hold π and 2π rotation of local magnetic moment in their structures, respectively. By employing the spin injection or spin transfer from such spin textures to a semiconductor 2DEG channel, the spatial structures in magnetic moments can be projected to the electron spins in semiconductors, leading to the formation of electron spin waves.

For the use of magnetic spin wave (magnon) to generate an electron spin wave, the collective precessional motion of local magnetic moments should be converted to spatial oscillations of electron spins. Spin pumping in a ferromagnet/nonmagnet structure is exploited as a tool for generating electron spin waves. The rotational motion of local magnetic moments under the ferromagnetic resonance condition

induces an a.c. spin current in a nonmagnet region.¹²³ If the nonmagnet is regarded as a semiconductor, by employing the drift transport for the injected a.c. spin current in a semiconductor, the spin polarization that varies periodically in time is converted to a periodic change of spin up and spin down in space, i.e., an electron spin wave. The induced periodicity, i.e., the wavelength of the electron spin wave, is controlled by resonant frequency and drift velocity.

For storing the wave-based information carriers in a nanomagnet, conversion from an electron spin wave to a magnetic spin wave (magnon) is indispensable. Spin absorption is a key to realize this conversion. In metallic systems, previous studies demonstrated that the magnetization switching in a nanomagnet can be achieved by the process of non-local spin injection and the following spin absorption,^{115,116} because the spin absorption generates a spin torque to the local magnetic moment. Such a control of magnetization by the spin absorption is also crucial for the conversion from an electron spin wave to a magnetic spin wave (magnon). In wave-based information carriers, we need the resonant excitation to select a particular mode of the magnetic spin wave (magnon) for spin-wave assisted switching. This means that a spin polarization that varies periodically in time is required in the spin current, which allows generation of an a.c.-type spin torque. The electron spin wave shows a periodic change in spin up and spin down in space. Thus, if one can transport the electron spin wave by a static electric field, i.e., by generating a drift current, under an external magnetic field parallel to the SO field and detect at a fixed position, this is regarded as a spin current with a time-variant spin polarization vector. We have roughly estimated the order of frequency for the induced a.c. spin current, which corresponds to 1–10 GHz using the following parameters based on Table I; the wavelength of the electron spin wave in a GaAs/AlGaAs QW is assumed to be 5 μm and the drift velocity is set at $(0.5\text{--}5) \times 10^4$ m/s. The frequency range is suitable to resonantly excite the magnetic spin wave (magnon) mode in a ferromagnet.⁵⁵ Of course, there is an issue to be solved. Compared to all-metallic systems,^{115,116} the efficiency of spin absorption is low because the magnitude of spin absorption depends on the spin resistance. According to a previous study on spin injection from a ferromagnetic metal electrode to a semiconductor channel,¹¹⁰ its high junction-resistance becomes a major obstacle for the efficient spin absorption. One of the possible solutions may be to employ a ferromagnetic semiconductor in order to reduce the junction resistance.¹⁰⁷

VII. CONCLUSION AND OUTLOOK

We have reviewed the concept of wave-parallel computing and have discussed basic properties and functionalities of electron spin waves and magnetic spin waves in view of applications as information carriers. We have also introduced Co-based Heusler alloy/GaAs 2DEG hybrid structures as a platform for generating and controlling electron spin waves and magnetic spin waves (magnon) and discussed their interconversions. By virtue of the spin-orbit induced effective magnetic field and its gate control in semiconductors, an electron spin wave exists stably as a persistent spin helix. It propagates over long distances by drift current. Multiple electron spin waves exist stably close to the persistent spin helix state. They are filtered using different decay time. These characteristics of electron spin waves are applicable within the framework of wave-parallel computing. To connect the electron spin wave to nonvolatile storage, magnetic spin wave (magnon)-assisted data writing has the potential to realize multi-state storage for information multiplexing. Because magnetic spin wave-assisted

magnetization switching occurs through the resonant excitation process of spin wave modes, it can achieve selective switching by transferring the spin angular momentum between an electron spin wave and a magnetic spin wave with identical frequencies. This switching requires efficient spin transfer between ferromagnet and semiconductor materials. The Co-based Heusler alloy/GaAs 2DEG hybrid structures allow the injection of a highly polarized spin current because of the half-metallic nature of Co-based Heusler alloys. Nevertheless, many technical issues must be resolved to support the functionalization of electron and magnetic spin waves and eventually to achieve realization of wave-parallel computing. Mixing and separation of electron spin waves should be demonstrated by experimentation. The demonstration of SD, SG, and U gate operations is an important step for constructing a general-purpose parallel computing architecture. Interconversion between electron spin waves and magnetic spin waves and the improvement of its efficiency are crucially important for using wave-based information processing and storage. Moreover, room-temperature operation of fundamental gates and interconversion are necessary. These issues provide plenty of room for future experiments exploiting the physics and application of electron spin wave and magnetic spin wave hybrid structures. Because multiplexity and parallelism are unique characteristics of waves that are distinct from current binary and sequential data processing and storage, spin-based wave-parallel computing might pave the way to handling the vast amount of information in future AI, IoT, and quantum information societies.

ACKNOWLEDGMENTS

M.K. thank to Professor J. Nitta, Dr. Iizasa, Dr. H. Sanada, Dr. Y. Kunihashi, Dr. H. Gotoh, Dr. T. Sogawa, Dr. P. Altmann, Dr. M. Kammermeier, Professor J. Ishihara, and Professor S. Yamamoto for fruitful discussion. M.K. was supported via a Grant-in-Aid for Scientific Research (Grant No. 21H04647) from the Japan Society for the Promotion of Science. This work was also supported by the JST FOREST and CREST programs (Grant Nos. JPMJFR203C and JPMJCR22C2).

AUTHOR DECLARATIONS

Conflict of Interest

The authors have no conflicts to disclose.

Author Contributions

Makoto Kohda: Conceptualization (lead); Writing – original draft (equal); Writing – review & editing (equal). **Takeshi Seki:** Conceptualization (equal); Writing – original draft (equal); Writing – review & editing (equal). **Yasushi Yuminaka:** Conceptualization (equal); Writing – original draft (equal); Writing – review & editing (equal). **Tetsuya Uemura:** Conceptualization (equal); Writing – original draft (equal); Writing – review & editing (equal). **Keito Kikuchi:** Data curation (equal). **Gian Salis:** Conceptualization (equal); Writing – original draft (equal); Writing – review & editing (equal).

DATA AVAILABILITY

The data that support the findings of this study are available from the corresponding author upon reasonable request.

REFERENCES

- ¹Semiconductor Spintronics and Quantum Computation Nanoscience and Technology Series, edited by D. D. Awschalom, D. Loss, and N. Samarth (Springer, Berlin 2022).
- ²T. Dietl, D. D. Awschalom, M. Kaminska, and H. Ohno, *Spintronics Semiconductors and Semimetals* (Academic, New York, 2008), Vol. 82.
- ³F. Pulizzi, *Nat. Mater.* **11**, 367–416 (2012).
- ⁴H. Hanyu, T. Endoh, D. Suzuki, H. Koike, Y. Ma, N. Onizawa, M. Natsui, S. Ikeda, and H. Ohno, *Proc. IEEE* **104**, 1844 (2016).
- ⁵Editorial, *Nat. Nanotechnol.* **10**, 185–226 (2015).
- ⁶*Spin Current* edited by S. Maekawa, S. O. Valenzuela, E. Saitoh, and T. Kimura (Oxford University Press, Oxford, 2015).
- ⁷Y. Taguchi, Y. Oohara, H. Yoshizawa, N. Nagaosa, and Y. Tokura, *Science* **291**, 2573–2576 (2001).
- ⁸Y. Machida, S. Nakatsuji, Y. Maeno, T. Tayama, T. Sakakibara, and S. Onoda, *Phys. Rev. Lett.* **98**, 057203 (2007).
- ⁹M. Heide, G. Bihlmayer, and S. Blügel, *Phys. Rev. B* **78**, 140403(R) (2008).
- ¹⁰A. Thiaville, S. Rohart, É. Jué, V. Cros, and A. Fert, *EPL* **100**, 57002 (2012).
- ¹¹S. Mühlbauer, B. Binz, F. Jonietz, C. Pfleiderer, A. Rosch, A. Neubauer, R. Georgii, and P. Böni, *Science* **323**, 915–919 (2009).
- ¹²C. Pappas, E. Lelièvre-Berna, P. Falus, P. M. Bentley, E. Moskvin, S. Grigoriev, P. Fouquet, and B. Farago, *Phys. Rev. Lett.* **102**, 197202 (2009).
- ¹³Y. Takeuchi, Y. Yamane, J.-Y. Yoon, R. Itoh, B. Jinnai, S. Kanai, J. Ieda, S. Fukami, and H. Ohno, *Nat. Mater.* **20**, 1364 (2021).
- ¹⁴F. Bloch, *Z. Phys.* **61**, 206–219 (1930).
- ¹⁵A. V. Chumak, V. I. Vasyuchka, A. A. Serga, and B. Hillebrands, *Nat. Phys.* **11**, 453–461 (2015).
- ¹⁶A. Khitun and K. L. Wang, *J. Appl. Phys.* **110**, 034306 (2011).
- ¹⁷S. Klingler, P. Pirro, T. Brächer, B. Leven, B. Hillebrands, and A. V. Chumak, *Appl. Phys. Lett.* **105**, 152410 (2014).
- ¹⁸O. Zografos, P. Raghavan, L. Amaru, B. Sorée, R. Lauwereins, I. Radu, D. Verkest, and A. Thean, in *IEEE/ACM International Symposium on Nanoscale Architectures* (IEEE, 2014), pp. 25–30.
- ¹⁹I. P. Radu, O. Zografos, A. Vaysset, F. Ciubotaru, M. Manfrini, P. Raghavan, S. Sayan, C. Adelmann, Z. Tókei, and A. Thean, in *IEEE International Interconnect Technology Conference/Advanced Metallization Conference* (IEEE, 2016), pp. 51–52.
- ²⁰S. Klingler, P. Pirro, T. Brächer, B. Leven, B. Hillebrands, and A. V. Chumak, *Appl. Phys. Lett.* **106**, 212406 (2015).
- ²¹A. Khitun, M. Bao, and K. L. Wang, *IEEE Trans. Magn.* **44**, 2141 (2008).
- ²²T. Brächer, F. Heussner, P. Pirro, T. Meyer, T. Fischer, M. Geilen, B. Heinz, B. Lägel, A. A. Serga, and B. Hillebrands, *Sci. Rep.* **6**, 38235 (2016).
- ²³K. Ganzhorn, S. Klingler, T. Wimmer, S. Geprägs, R. Gross, H. Huebl, and S. T. B. Goennenwein, *Appl. Phys. Lett.* **109**, 022405 (2016).
- ²⁴O. Zografos, S. Dutta, M. Manfrini, A. Vaysset, B. Sorée, A. Naeemi, P. Raghavan, R. Lauwereins, and I. P. Radu, *AIP Adv.* **7**, 056020 (2017).
- ²⁵A. Mahmoud, F. Vanderveken, C. Adelmann, F. Ciubotaru, S. Hamdioui, and S. Cotofana, *AIP Adv.* **10**, 035119 (2020).
- ²⁶T. Fischer, M. Kewenig, D. A. Bozhko, A. A. Serga, I. I. Syvorotka, F. Ciubotaru, C. Adelmann, B. Hillebrands, and A. V. Chumak, *Appl. Phys. Lett.* **110**, 152401 (2017).
- ²⁷G. Talmelli, T. Devolder, N. Träger, J. Förster, S. Wintz, M. Weigand, H. Stoll, M. Heyns, G. Schütz, I. P. Radu, J. Gräfe, F. Ciubotaru, and C. Adelmann, *Sci. Adv.* **6**, eabb4042 (2020).
- ²⁸N. Kanazawa, T. Goto, K. Sekiguchi, A. B. Granovsky, C. A. Ross, H. Takagi, Y. Nakamura, H. Uchida, and M. Inoue, *Sci. Rep.* **7**, 7898 (2017).
- ²⁹Q. Wang, M. Kewenig, M. Schneider, R. Verba, F. Kohl, B. Heinz, M. Geilen, M. Mohseni, B. Lägel, F. Ciubotaru, C. Adelmann, C. Dubs, S. D. Cotofana, O. V. Dobrovolskiy, T. Brächer, P. Pirro, and A. V. Chumak, *Nat. Electron.* **3**, 765–774 (2020).
- ³⁰A. Mahmoud, F. Ciubotaru, F. Vanderveken, A. V. Chumak, S. Hamdioui, C. Adelmann, and S. Cotofana, *J. Appl. Phys.* **128**, 161101 (2020).
- ³¹G. Dresselhaus, *Phys. Rev.* **100**, 580 (1955).
- ³²E. I. Rashba, *Fiz. Tverd. Tela* **2**, 1224 (1960).
- ³³R. Winkler, *Spin-Orbit Coupling Effects in Two-Dimensional Electron and Hole Systems* (Springer-Verlag, Berlin, 2003), Vol. 191.

- ³⁴M. I. Dyakonov and V. I. Perel', Sov. Phys. JETP **33**, 1053 (1971).
- ³⁵B. A. Bernevig, J. Orenstein, and S.-C. Zhang, Phys. Rev. Lett. **97**, 236601 (2006).
- ³⁶J. Schliemann, J.-C. Egues, and D. Loss, Phys. Rev. Lett. **90**, 146801 (2003).
- ³⁷J. D. Koralek, C. P. Weber, J. Orenstein, B. A. Bernevig, S.-C. Zhang, S. Mack, and D. D. Awschalom, Nature **458**, 610 (2009).
- ³⁸M. Kohda and G. Salis, Semicond. Sci. Technol. **32**, 073002 (2017).
- ³⁹J. Schliemann, Rev. Mod. Phys. **89**, 011001 (2017).
- ⁴⁰M. P. Walser, C. Reichl, W. Wegscheider, and G. Salis, Nat. Phys. **8**, 757 (2012).
- ⁴¹M. Kohda, V. Lechner, Y. Kunihashi, T. Dollinger, P. Olbrich, C. Schönhuber, I. Caspers, V. V. Bel'kov, L. E. Golub, D. Weiss, K. Richter, J. Nitta, and S. D. Ganichev, Phys. Rev. B **86**, 081306(R) (2012).
- ⁴²Y. Kunihashi, H. Sanda, H. Gotoh, K. Onomitsu, M. Kohda, J. Nitta, and T. Sogawa, Nat. Commun. **7**, 10722 (2016).
- ⁴³S. Anghel, F. Passmann, K. J. Schiller, J. N. Moore, G. Yusa, T. Mano, T. Noda, M. Betz, and A. D. Bristow, Phys. Rev. B **101**, 155414 (2020).
- ⁴⁴C. Schönhuber, M. P. Walser, G. Salis, C. Reichl, W. Wegscheider, T. Korn, and C. Schüller, Phys. Rev. B **89**, 085406 (2014).
- ⁴⁵J. Ishihara, Y. Ohno, and H. Ohno, Appl. Phys. Express **7**, 013001 (2014).
- ⁴⁶A. Sasaki, S. Nonaka, Y. Kunihashi, M. Kohda, T. Bauernfeind, T. Dollinger, K. Richter, and J. Nitta, Nat. Nanotechnol. **9**, 703 (2014).
- ⁴⁷N. Yamaguchi and F. Ishii, Appl. Phys. Express **10**, 123003 (2017).
- ⁴⁸F. Passmann, S. Anghel, T. Tischler, A. V. Poshakinskiy, S. A. Tarasenko, G. Karczewski, T. Wojtowicz, A. D. Bristow, and M. Betz, Phys. Rev. B **97**, 201413(R) (2018).
- ⁴⁹L. L. Tao and E. Y. Tsymbal, Nat. Commun. **9**, 2763 (2018).
- ⁵⁰C. Autieri, P. Barone, J. Ślawińska, and S. Picozzi, Phys. Rev. Mater. **3**, 084416 (2019).
- ⁵¹M. A. U. Absor and F. Ishii, Phys. Rev. B **100**, 115104 (2019).
- ⁵²H. Ai, X. Ma, X. Shao, W. Li, and M. Zhao, Phys. Rev. Mater. **3**, 054407 (2019).
- ⁵³Spin Physics in Semiconductors Second, edited by M. I. Dyakonov (Springer, Berlin, 2017).
- ⁵⁴D. Chiba, Y. Sato, T. Kita, F. Matsukura, and H. Ohno, Phys. Rev. Lett. **93**, 216602 (2004).
- ⁵⁵A. V. Chumak, A. A. Serga, and B. Hillebrands, J. Phys. D: Appl. Phys. **50**, 244001 (2017).
- ⁵⁶R. Bez, E. Camerlenghi, A. Modelli, and A. Visconti, Proc. IEEE **91**, 489–502 (2003).
- ⁵⁷T. Aoki and T. Higuchi, Interdiscip. Inf. Sci. **1**, 1–18 (1994).
- ⁵⁸T. Aoki, Y. Yuminaka, and T. Higuchi, IEE Proc. G **140**, 191–198 (1993).
- ⁵⁹Y. Yuminaka, T. Aoki, and T. Higuchi, IEICE Trans. Electron. E76-C, 1133–1143 (1993); available at URL is as follows: https://search.ieice.org/bin/summary.php?id=e76-c_7_1133.
- ⁶⁰G. Engels, J. Lange, T. Schäpers, and H. Lüth, Phys. Rev. B **55**, R1958 (1997).
- ⁶¹J. Nitta, T. Akazaki, H. Takayanagi, and T. Enoki, Phys. Rev. Lett. **78**, 1335 (1997).
- ⁶²M. P. Walser, U. Siegenthaler, V. Lechner, D. Schuh, S. D. Ganichev, W. Wegscheider, and G. Salis, Phys. Rev. B **86**, 195309 (2012).
- ⁶³F. Dettwiler, J. Fu, S. Mack, P. J. Weigle, J. C. Egues, D. D. Awschalom, and D. M. Zumbühl, Phys. Rev. X **7**, 031010 (2017).
- ⁶⁴M. Kohda and J. Nitta, Phys. Rev. B **81**, 115118 (2010).
- ⁶⁵D. Grundler, Phys. Rev. Lett. **84**, 6074 (2000).
- ⁶⁶Y. Lin, T. Koga, and J. Nitta, Phys. Rev. B **71**, 045328 (2005).
- ⁶⁷K. Yoshizumi, A. Sasaki, M. Kohda, and J. Nitta, Appl. Phys. Lett. **108**, 132402 (2016).
- ⁶⁸T. Nishimura, K. Yoshizumi, T. Saito, D. Iizasa, J. Nitta, and M. Kohda, Phys. Rev. B **103**, 094412 (2021).
- ⁶⁹M. Scheid, M. Kohda, Y. Kunihashi, K. Richter, and J. Nitta, Phys. Rev. Lett. **101**, 266401 (2008).
- ⁷⁰D. Iizasa, M. Kohda, U. Zulicke, J. Nitta, and M. Kammermeier, Phys. Rev. B **101**, 245417 (2020).
- ⁷¹Y. S. Chen, S. Fält, W. Wegscheider, and G. Salis, Phys. Rev. B **90**, 121304(R) (2014).
- ⁷²P. Altmann, M. Kohda, C. Reichl, W. Wegscheider, and G. Salis, Phys. Rev. B **92**, 235304 (2015).
- ⁷³P. Altmann, M. P. Walser, C. Reichl, W. Wegscheider, and G. Salis, Phys. Rev. B **90**, 201306 (2014).
- ⁷⁴M. Schwemmer, A. Hanninger, M. Weingartner, M. Oltscher, M. Ciorga, D. Weiss, D. Schuh, D. Bougeard, T. Korn, and C. Schüller, Appl. Phys. Lett. **106**, 172106 (2016).
- ⁷⁵T. Saito, T. Nishimura, J.-Y. Yoon, J. Kölzer, D. Iizasa, M. Kammermeier, T. Schäpers, J. Nitta, and M. Kohda, Phys. Rev. Res. **4**, 043217 (2022).
- ⁷⁶P. Kleinert and V. V. Bryksin, Phys. Rev. B **76**, 205326 (2007).
- ⁷⁷L. Yang, J. Orenstein, and D.-H. Lee, Phys. Rev. B **82**, 155324 (2010).
- ⁷⁸G. Salis, M. P. Walser, P. Altmann, C. Reichl, and W. Wegscheider, Phys. Rev. B **89**, 045304 (2014).
- ⁷⁹M. Kohda, T. Seki, Y. Yuminaka, and T. Uemura, Multiplex transmission and separation detection method of electron spin wave, PCT/JP2022/018255 (2022).
- ⁸⁰R. E. Rottmayer, S. Batra, D. Buechel, W. A. Challener, J. Hohlfeld, Y. Kubota, L. Li, B. Lu, C. Mihalcea, K. Mountfield, K. Pelhos, C. Peng, T. Rausch, M. A. Seigler, D. Weller, and X. Yang, IEEE Trans. Magn. **42**, 2417 (2006).
- ⁸¹S. Okamoto, N. Kikuchi, M. Furuta, O. Kitakami, and T. Shimatsu, J. Phys. D: Appl. Phys. **48**, 353001 (2015).
- ⁸²T. Seki, K. Utsumiya, Y. Nozaki, H. Imamura, and K. Takanashi, Nat. Commun. **4**, 1726 (2013).
- ⁸³T. Seki, K. Hotta, H. Imamura, Y. Nozaki, and K. Takanashi, Appl. Phys. Lett. **103**, 122403 (2013).
- ⁸⁴T. Seki, W. Zhou, and K. Takanashi, J. Phys. D: Appl. Phys. **49**, 075002 (2016).
- ⁸⁵W. Zhou, T. Yamaji, T. Seki, H. Imamura, and K. Takanashi, Appl. Phys. Lett. **110**, 082401 (2017).
- ⁸⁶D. C. Ralph and M. D. Stiles, J. Magn. Magn. Mater. **320**, 1190 (2008).
- ⁸⁷W. Zhou, T. Seki, H. Arai, H. Imamura, and K. Takanashi, Phys. Rev. B **94**, 220401 (2016).
- ⁸⁸W. Zhou, T. Seki, and K. Takanashi, J. Appl. Phys. **122**, 093902 (2017).
- ⁸⁹R. Fiederling, M. Keim, G. Reuscher, W. Ossau, G. Schmidt, A. Waag, and L. W. Molenkamp, Nature **402**, 787 (1999).
- ⁹⁰X. Jian, R. Wang, R. M. Shelly, R. M. Macfarlane, S. R. Bank, J. S. Harris, and S. S. P. Parkin, Phys. Rev. Lett. **94**, 056601 (2005).
- ⁹¹P. Van Dorpe, Z. Liu, W. Van Roy, V. F. Motsnyi, M. Sawicki, G. Borghs, and J. De Boeck, Appl. Phys. Lett. **84**, 3495 (2004).
- ⁹²M. Kohda, T. Kita, Y. Ohno, F. Matsukura, and H. Ohno, Appl. Phys. Lett. **89**, 012103 (2006).
- ⁹³M. Ciorga, A. Einwanger, U. Wurstbauer, D. Schuh, W. Wegscheider, and D. Weiss, Phys. Rev. B **79**, 165321 (2009).
- ⁹⁴M. Ciorga, M. Utz, D. Schuh, D. Bougeard, and D. Weiss, Phys. Rev. B **88**, 155308 (2013).
- ⁹⁵F. Eberle, D. Schuh, B. Grünewald, D. Bougeard, D. Weiss, and M. Ciorga, Nano Lett. **23**, 4815 (2023).
- ⁹⁶J. Kübler, A. R. Williams, and C. B. Sommers, Phys. Rev. B **28**, 1745 (1983).
- ⁹⁷S. Ishida, S. Fujii, S. Kashiwagi, and S. Asano, J. Phys. Soc. Jpn. **64**, 2152 (1995).
- ⁹⁸S. Picozzi, A. Continenza, and A. J. Freeman, Phys. Rev. B **66**, 094421 (2002).
- ⁹⁹I. Galanakis, P. H. Dederichs, and N. Papanikolaou, Phys. Rev. B **66**, 174429 (2002).
- ¹⁰⁰P. J. Webster, J. Phys. Chem. Solids **32**, 1221 (1971).
- ¹⁰¹X. Y. Dong, C. Adelmann, J. Q. Xie, C. J. Palmström, X. Lou, J. Strand, P. A. Crowell, J.-P. Barnes, and A. K. Petford-Long, Appl. Phys. Lett. **86**, 102107 (2005).
- ¹⁰²M. C. Hickey, C. D. Damsgaard, I. Farrer, S. N. Holmes, A. Husmann, J. B. Hansen, C. S. Jacobsen, D. A. Ritchie, R. F. Lee, G. A. C. Jones, and M. Pepper, Appl. Phys. Lett. **86**, 252106 (2005).
- ¹⁰³M. Ramsteiner, O. Brandt, T. Flissikowski, H. T. Grahn, M. Hashimoto, J. Herfort, and H. Kostial, Phys. Rev. B **78**, 121303(R) (2008).
- ¹⁰⁴P. Bruski, Y. Manzke, R. Farshchi, O. Brandt, J. Herfort, and M. Ramsteiner, Appl. Phys. Lett. **103**, 052406 (2013).
- ¹⁰⁵T. A. Peterson, S. J. Patel, C. C. Geppert, K. D. Christie, A. Rath, D. Pennachio, M. E. Flatté, P. M. Voyles, C. J. Palmström, and P. A. Crowell, Phys. Rev. B **94**, 235309 (2016).
- ¹⁰⁶T. Saito, N. Tezuka, M. Matsura, and S. Sugimoto, Appl. Phys. Express **6**, 103006 (2013).
- ¹⁰⁷M. Oltscher, M. Ciorga, M. Utz, D. Schuh, D. Bougeard, and D. Weiss, Phys. Rev. Lett. **113**, 236602 (2014).

- ¹⁰⁸H. C. Koo, J. H. Kwon, J. Eom, J. Chang, S. H. Han, and M. Johnson, *Science* **325**, 1515–1518 (2009).
- ¹⁰⁹Y. Ebina, T. Akiho, H-x Liu, M. Yamamoto, and T. Uemura, *Appl. Phys. Lett.* **104**, 172405 (2014).
- ¹¹⁰Z. Lin, D. Pan, M. Rasly, and T. Uemura, *Appl. Phys. Lett.* **114**, 012405 (2019).
- ¹¹¹T. Uemura, T. Akiho, M. Harada, K. Matsuda, and M. Yamamoto, *Appl. Phys. Lett.* **99**, 082108 (2011).
- ¹¹²Y. Tserkovnyak, A. Brataas, and G. E. W. Bauer, *Phys. Rev. Lett.* **88**, 117601 (2002).
- ¹¹³S. Mizukami, Y. Ando, and T. Miyazaki, *Phys. Rev. B* **66**, 104413 (2002).
- ¹¹⁴E. Saitoh, M. Ueda, and H. Miyajima, *Appl. Phys. Lett.* **88**, 182509 (2006).
- ¹¹⁵T. Kimura, Y. Otani, and J. Hamrle, *Phys. Rev. Lett.* **96**, 037201 (2006).
- ¹¹⁶T. Yang, T. Kimura, and Y. Otani, *Nat. Phys.* **4**, 851 (2008).
- ¹¹⁷L. Q. Liu, T. Moriyama, D. C. Ralph, and R. A. Buhrman, *Phys. Rev. Lett.* **106**, 036601 (2011).
- ¹¹⁸L. Q. Liu, O. J. Lee, T. J. Gudmundsen, D. C. Ralph, and R. A. Buhrman, *Phys. Rev. Lett.* **109**, 096602 (2012).
- ¹¹⁹A. Fuhrer and G. Salis, US Patent US 9001574 B2 (2013).
- ¹²⁰A. Forbes, M. De Oliveira, and M. R. Dennis, *Nat. Photonics* **15**, 253–262 (2021).
- ¹²¹C. He, Y. Shen, and A. Forbes, *Light: Sci. Appl.* **11**, 205 (2022).
- ¹²²J. Ishihara, T. Mori, T. Suzuki, S. Sato, K. Morita, M. Kohda, Y. Ohno, and K. Miyajima, *Phys. Rev. Lett.* **130**, 126701 (2023).
- ¹²³D. Wei, M. Obstbaum, M. Ribow, C. H. Back, and G. Woltersdorf, *Nat. Commun.* **5**, 3768 (2014).